AFOSR-TR-95

0581

Development and Assessment
of Turbulence-Chemistry Models
in Highly Strained Non-Premixed Flames

Final Report

DTIC
SELECTED
OCT 1 3 1995
F

Approved
distribu.

per

USAF, AFSC
Air Force Office of Scientific Research
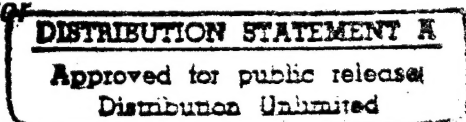**110 Duncan Avenue, Suite B115**
Bolling Air Force Base, DC 20332

19951012 055

Principal Investigator
Sanjay M. Correa

October 1994

DTIC QUALITY INSPECTED 5

REPORT DOCUMENTATION PAGE

Form Approved
OMB No. 0704-0188

1. AGENCY USE ONLY (*Leave blank*)	2. REPORT DATE 31 October 1994	3. REPORT TYPE AND DATES COVERED Final Report for 1 Oct 1991 to 30 Sep 1994

4. TITLE AND SUBTITLE

(U) Development And Assessment Of Turbulence-Chemistry Models In Highly Strained Non-premixed Flames

5. FUNDING NUMBERS

PE-61102F
PR-2308
SA-BS
G-F49620-91-C-0072

6. AUTHOR(S)

Sanjay M. Correa

7. PERFORMING ORGANIZATION NAME(S) AND ADDRESS(ES)

General Electric Corporate Research and Development Center
P.O. Box 8, K1-ES210
Schenectady, NY 12301

8. PERFORMING ORGANIZATION REPORT NUMBER

94SRD008

9. SPONSORING/MONITORING AGENCY NAME(S) AND ADDRESS(ES)

AFOSR/NA
110 Duncan Avenue, Suite B115
Bolling AFB, DC, 20332-0001

10. SPONSORING/MONITORING AGENCY REPORT NUMBER

11. SUPPLEMENTARY NOTES

12a. DISTRIBUTION/AVAILABILITY STATEMENT

Approved for public release; Distribution unlimited

12b. DISTRIBUTION CODE

UL

13. ABSTRACT *(Maximum 200 words)*

The goal of this research is a quantitative understanding of turbulence-chemistry interactions as they pertain to combustion in aeropropulsion engines. The two principal classes of accomplishment are:

(1) The first-ever stochastic joint velocity-composition pdf simulations of bluff-body stabilized flames, and comparison with Raman data on major species, temperature and mixture fraction (mean and rms quantities of each) in the same burner. Fuels have been CO/H_2 mixtures (whose reduced chemistry is modeled with two compositional variables) and methane (five variables). This method of merging pdf transport and CFD codes can be used to combine the pdf model with any of the CFD codes used in design. There is thus a clear path for transitioning the results of the research. Remaining issues included (i) a chemistry scheme for jet fuels (not just CO/H_2 and CH_4), tested in turbulence and not only in the the laminar context, and (ii) more species and temperature data in the regime of high turbulence intensity, so that the model can be tested in the regime of real engines.

(2) The "Partially Stirred Reactor" or PaSR model was developed toward the first two of these goals. The unsteady evolution of a full chemistry scheme is computed in the presence of turbulence of prescribed frequency. The model has been used to study the amplitude of fluctuations in temperature or species, the performance of reduced versus full chemistry schemes and of mixing models versus each other, as functions of the turbulence all the way to blowout at gas-turbine conditions. The PaSR is a better prototype of turbulent combustion than is the classical strained laminar flame. The PaSR is shown both formally and by actual numerical simulations to tend to a PSR in the limit of infinite mixing frequency. The fuels simulated were CO/H2 (43 reactions), methane (77 reactions), and a general higher hydrocarbon initiated by a pyrolysis step. Reduced schemes were found to be acceptable within limits which were more precisely determined than in prior analyses. Mixing models were found to be similar at high mixing frequencies but to be different at low mixing frequencies. These results have standalone value (only tool for full chemistry plus turbulence) and also feed into pdf/CFD calculations.

14. SUBJECT TERMS

Turbulent combustion; Monte Carlo pdf model; finite-rate chemistry; reduced schemes; bluff-body flames; scalar mixing.

15. NUMBER OF PAGES
55

16. PRICE CODE

17. SECURITY CLASSIFICATION OF REPORT: UNCLASSIFIED	18. SECURITY CLASSIFICATION OF THIS PAGE: UNCLASSIFIED	19. SECURITY CLASSIFICATION OF ABSTRACT: UNCLASSIFIED	20. LIMITATION OF ABSTRACT UL

TABLE OF CONTENTS

Accesion For

NTIS   CRA&I   ☑
DTIC   TAB   ☐
Unannounced   ☐
Justification

By

Distribution /

Availability Codes

Dist   Avail and / or
        Special

A-1

LIST OF ILLUSTRATIONS

(a) Mean temperature.

(b) Mean fuel mass fraction.

(c) Mean Y^*, combined variable based on the CO and H_2 mole numbers.

NOMENCLATURE

C_ϕ	constant in mixing model
Da	Damkohler number
g	scalar variance; gravitational acceleration
h	species enthalpy
H	particle enthalpy
J	molecular flux
k	turbulence kinetic energy; reaction rate
m	mass flow rate into reactor
m_p	particle mass
M_k	molecular weight of species k
N_{in}	number of particles flowing in per time step
N_p	number of particles in ensemble
N_s	number of species
p	pressure
P	probability density function
S	reaction rate
t	time
T	temperature
u	velocity component
V	reactor volume; velocity vector
w	molar production rate per unit volume
W	molecular weight
x	spatial coordinate
Y_k	mass fraction of species k
Z	elemental mass fraction
α	weighting coefficient
ξ	mixture fraction
ε	dissipation rate of turbulence kinetic energy
ϱ	density
σ	mole number
τ	reactor residence time; stress tensor
Φ	fuel−air equivalence ratio
ψ	particle age; compositional vector
ω	mixing frequency

Superscripts

a   air

e   equilibrium

f   fuel

(n)   index of nth particle

u   unburned (frozen)

$\overline{\phi}$, $<\phi>$ ensemble average of quantity ϕ

Subscripts

in   inlet conditions

k   index of kth species

s   stoichiometric

*   combined variable

Section 1

SUMMMARY

This final report describes work performed in the period October 1991 to September 1994 for the U.S. Air Force of Scientific Research under Contract No. F49620−91−C−0072. Dr. Julian Tishkoff was the AFOSR Project Monitor. The work was performed and the report has been prepared by the Mechanical Systems Laboratory at the GE Corporate Research and Development Center, Schenectady, New York. This section summarizes the technical problem which was considered. The conclusions are summarized in Section 3.

Aeropropulsion gas−turbines generally employ non−premixed turbulent combustion. These engines have aggressive design objectives − including supercruise, increasing thrust:weight ratio, low observables in the exhaust, higher altitude performance, endothermic fuel capability, and low pollutant emissions − which in turn lead to new challenges for the combustion system: decreasing size, increasing combustor temperature rise, and low emissions of pollutants, smoke and other visibles. Chemical kinetics and their interactions with turbulence control these phenomena. Although the hypothesis of fast chemistry or "mixed−is−burned" is useful for understanding traditional design issues such as equilibrium exit temperature fields ("pattern factor"), it cannot address these challenges. The goal of this three−year research program was a quantitative understanding of turbuence−chemistry interactions in the above systems.

Computational modeling is playing an increasingly large role because of the high cost of prototype development and testing. Today, products are planned and sales efforts are launched on the basis of <u>predicted</u> performance, and metal is not actually cut until customers are lined up. Models must therefore address all the issues of concern to customers, as outlined above. This is a more ambitious set of parameters than the traditional requirement of only the pattern factor.

Because the principal task of the combustor is to deliver hot combustion products to the turbine, mixing alone or chemistry alone are not sufficient criteria by which to judge performance. <u>Mixing</u> and <u>chemistry</u> are <u>simultaneous</u>. For example, the large−scale unsteadiness sometimes seen in combustors is often taken as evidence that the in−flame mixing is so slow that it becomes process−limiting; however, there are other factors at play. The combustor cannot deliver an unsteady flow to the turbines or else they will be damaged; hence the exit temperature and velocity fields must be steady and mixed. Also, much of the important minor species chemistry is too slow to be affected. The Damkohler numbers (ratios of mixing to chemical times for all important mixing scales and all important reactions) are an excellent way to characterize the effect of mixing in the context of chemistry. Our program has shown that in aeropropulsion combustors most important Damkohler numbers are in the distributed reaction regime. This includes disparate phenomena such as flame stability (e.g., good reproduction of blowout limits) and CO or NO_x emissions.

Our research program addressed the technical issues by the development (and detailed validation) of computational models that <u>fit</u> <u>into</u> <u>a</u> <u>familiar</u> <u>framework</u>. Otherwise the design and development communities would not be able to use the results. It also seems clear that different modeling approaches will be needed to address different issues. Unsteady methods such as Large Eddy Simulation or Discrete Vortex Models may be used to isolate features of the flowfield, such as mixing layers. Direct Numerical Simulation will play a role in physical sub−model development. These methods, however, will not directly transfer information to the majority of engineers. The present pdf method with a selected reduced chemistry scheme

1

— the latter having been tested versus full chemistry in <u>turbulent</u> and not laminar combustion — is superior to others <u>in</u> <u>the</u> <u>context</u> <u>of</u> <u>gas—turbine</u> <u>combustion.</u>

Statement of Work

<u>Task 1:</u> Literature survey of well—characterized bluff—body stabilized turbulent non—premixed flames. Experiments with laser—based spectroscopic data, particularly Raman/CARS and fluorescence, on critical quantities will be favored. Compilation of data. Recommendations for future experiments. (Leading candidates were the University of Sydney/SANDIA "Reverse Flow Reactor," the GE bluff—body stabilized burner used in the current AFOSR program, the ALTEX/SANDIA burner and the Air Force Aeropropulsion Laboratory burner.) Recent literature on piloted jet flames will also be surveyed for data in the regime of intense turbulence.

Sections 2.1 and 2.2 describe the work.

<u>Task 2:</u> Formulation and discretization of equations for selected turbulence—chemistry sub—models, in elliptic form appropriate for steady—state multi—dimensional computation. The sub—models include:

> 1. The laminar flamelet model with a model for scalar dissipation rate and with full chemistry.
> 2. Assumed shape pdf method with lower moments from balance equations and with reduced chemistry schemes.
> 3. Direct Monte—Carlo pdf evolution methods for the scalar pdf, with reduced chemistry schemes.
> 4. Hybrid partial equilibrium—flamelet approach, which treats slow (e.g., recombination) reactions in a distributed zone mode and and fast (e.g., chain—branching) reactions in a flamelet mode.
> 5. Semi—empirical approach which treats the fine scales as a perfectly stirred reactor, with mass flux into this regime based on dimensional analysis.
> 6. Models which may emerge as research progresses at GE and elsewhere.
> The basic flow algorithm can be modified in each case, as required to cater to the particular sub—model, but in general will have second—order (in sense of stress/flux correlations) closure on turbulence and second—order accurate (in sense of Taylor series truncation error) discretization.

Picking up on the theme that <u>mixing</u> <u>and</u> <u>chemistry</u> <u>are</u> <u>simultaneous,</u> a new tool for the simulation of the interaction between (simultaneous) prescribed turbulence and full chemistry schemes has been developed. We argue that it is superior to other tools such as the strained laminar flame or the PSR. It also traces a direct lineage from pdf/CFD models as shown below. Sections 2.1 and 2.4 describe the work.

<u>Task 3:</u> Assessment of each of the selected turbulence—chemistry sub—models against each of the selected datasets. Comparisons of the following types of quantities as available in each case:

> 1. Mean velocity and turbulence fields.
> 2. Mean major species and temperature.
> 3. Fluctuations (e.g., variance) in major species and temperature.
> 4. Mean minor species.
> 5. Fluctuations (e.g., variance) in minor species
> 6. Important covariances.

Sections 2.2 and 2.5—2.8 describe the work.

Section 2

TECHNICAL DISCUSSION

Despite significant progress, it is not clear how turbulent combustion should be viewed. Conceptual questions arise such as whether turbulent flames act as ensembles of strained laminar "flamelets" or as broader "distributed" zones of reacting species. Engineering models of combustors rely largely on simple approaches such as fast chemistry (mixed is burned) and assumed shape probability density functions (pdf's), and have been successful in terms of gross features such as the profiles of combustor exit temperature. Present−day demands on combustion equipment and thus on computational models are, however, increasing the need for advanced understanding of turbulence−chemistry interactions. For example, (i) flameout and relight in turbine combustors are related to interactions with chain−branching reactions, (ii) hydrogen burnout in supersonic combustors is related to interactions with recombination reactions, and (iii) requirements of low emissions of NO_x, CO, smoke, and other observables are related to non−equilibria among species such as oxyhydrogen radicals and C_xH_y. These turbulence−chemistry interactions span several orders of magnitude in Damkohler number, depending on the specific reaction and the specific turbulence process in question.

New models for turbulence−chemistry interactions in air−breathing combustion have been developed and compared with turbulent flame data. Accomplishments in the reporting period include:
(1) Development of the hybrid Monte Carlo joint PDF/CFD model for a bluff−body stabilized flame. Detailed comparisons have been made with Raman data on means and rms of mixture fraction, major species and temperature in non−premixed bluff−body stabilized $CO/H_2/N_2$ and CH_4 flames;
(2) Development of the "PaSR" or partially stirred reactor. The PaSR offers an alternative to traditional evaluations in laminar flames, which are not relevant to turbulent combustion. Reduced CO/H_2 schemes and reduced methane schemes are compared with full schemes in the PaSR model. These studies span several decades of turbulent mixing frequency. A three−variable reduced scheme for complex hydrocarbon fuels is compared in the PaSR with the starting scheme over two decades of turbulence frequency. Direct comparisons of different mixing models are conducted in the context of a full chemistry scheme.

The following sub−sections highlight the approach and the results.

2.1 Experimental Set−Up and Hybrid Monte Carlo Joint PDF/CFD Modeling

The pressure−corrected mean Navier−Stokes/assumed−shape pdf/k−ε turbulence model does not account rigorously for the turbulence−chemistry interactions of dominant interest, but affords significant geometric flexibility and rapid convergence for pressure−dominated internal flow [Correa and Shyy (1987)]. On the other hand, the joint (velocity−composition) pdf transport model includes turbulence and chemistry with single−point closure [Pope (1990)]. The pdf model has been widely used to compute turbulent jet flames, both in the composition−only form [Chen and Kollmann (1989)] and in the joint velocity−composition form [Pope and Correa (1986)]. More recently, the joint pdf model has been extended to "elliptic" (recirculating) flow and applied to the computation of CO/H_2 bluff−body flames [Correa and Pope (1992, 1994)], marking a step toward the recirculation−stabilized flowfields found in practical burners. Bluff bodies also eliminate the pilot−stabilization necessary in jet flames at high Reynolds numbers.

There are other approaches, intermediate in complexity and cost, between the assumed shape pdf model (#1) and the joint velocity−composition pdf transport model (#4). The "conditional moment clo-

3

sure" model (#2) solves conventional time−averaged field equations for the means of reactive scalars conditioned on the mixture fraction [Smith et al. (1992)], and is applicable only when fluctuations about this conditional mean are small. The scalar pdf model (#3) does not treat the velocity part of the pdf, using instead conventional turbulence modeling to supply the scalar (and momentum) fluxes [Chen et al. (1989)]. Arguments of computational cost are usually made to support models #1−#3; however, the speedup achieved in parallelizing particle tracking pdf computations (accomplished in the present reporting period of this contract) shows that the pdf computations are tractable in practical design codes [Correa and Braaten (1993)].

Methane is of particular interest in this context: (1) for scientific reasons because it affords strong finite−rate chemistry effects and well−studied reduced kinetic schemes, and (2) for practical reasons because there is a significant worldwide natural gas economy. For example, about 50 GW of new gas−fired powerplants are being sold annually. The development and qualification of predictive tools (with the required geometry, chemistry, and turbulence capabilities) will aid this industry. We will not report in detail on the CO/H_2 flame, because the methane flame was more challenging. The CO/H_2 flame has been reported in the archival literature [Correa and Pope (1992)].

Of the many prior bluff−body flame studies, the most closely related is that of Masri et al. (1992) who also used fluorescence−corrected Raman spectroscopy of methane−air flames. The present work uses a jet which is twice as big and stresses the jet−dominated regime, which is less susceptible to large−scale shedding off the bluff body; greater degrees of extinction are found. Hence, the new contributions are Raman temperature and major species measurements in the jet−dominated regime of a bluff−body stabilized non−premixed methane−air flame.

The bluff body burner and the inflow conditions are shown in Fig. 1. The axisymmetric bluff body has an outer diameter of 38.1 mm. with an axial jet of diameter "d" 3.18 mm. located in the center. It is well known that parts of this flowfield (notably, the annular shear layer shed off the bluff body) can be dominated by unsteady effects. Care was taken to operate in a velocity (jet and coflow) regime where the flame was steady. The cold jet Reynolds number is 12,000, based on the jet diameter and jet exit velocity of 62.5 m/s. The coflow air velocity is 18 m/s. The back surface of the bluff body is coated with a thermal barrier material to reduce heat loss. The flame is stabilized by the recirculation zone provided by the bluff body. The tunnel cross section is 15 cm x 15 cm, large enough not to interfere with the flame. (The calculations are made for a circular duct of the same cross−sectional area). Visual observations of methane flames at various air and fuel jet velocities were used to select the conditions for the Raman−scattering measurements reported below. This flame is anchored by the bluff body and is almost extinguished in the neck region, before re−igniting further downstream.

The Raman system is based on a flashlamp pumped dye laser which provides pulses of $\approx$ 1J in 2−4 μs, within a 0.2 nm bandpass at 488 nm at a repetition rate of 10 Hz. The light scattered at right angles is collected by two lenses, separated in frequency by a 3/4 m spectrometer and is detected by eight photomultiplier tubes. The photomultiplier tubes detect anti−Stokes vibrational Raman scattering from N_2, Stokes vibrational Raman scattering from N_2, O_2, H_2, H_2O, CO and CO_2, and Rayleigh scattering. The temporal resolution (2−4 μs) of the technique is limited by the laser pulse length, the spatial resolution (0.2 x 0.2 x 0.6 mm) is limited by the spectrometer entrance slit and the collection optics, and the data acquisition rate is limited by the laser repetition rate. The flame luminescence was broad−banded throughout the visible re-

4

gion, and was reduced by a polarization filter in the collection optics. The polarization vector was aligned to pass horizontally polarized Raman– and Rayleigh–scattered light.
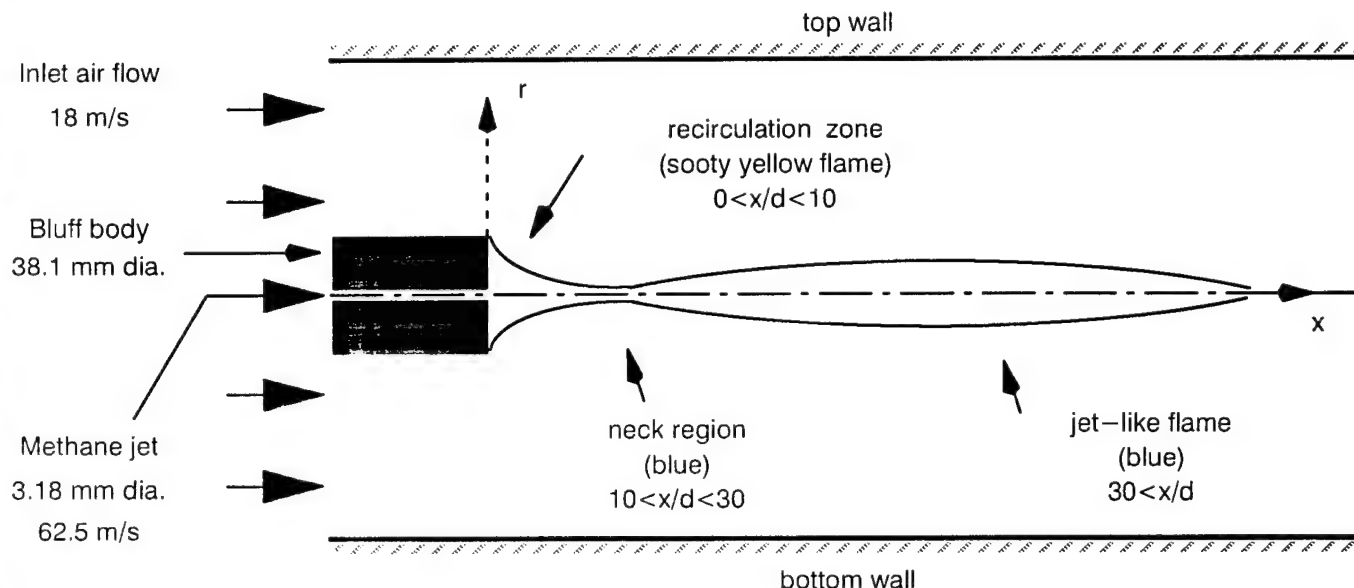

Figure 1. Non–premixed bluff–body–stabilized methane flame; "d" is the jet diameter.

The instantaneous temperature on every laser shot was determined in three independent ways: (1) the Stokes–anti–Stokes (SAS) ratio from N_2, which yields the temperature directly [Drake et al. (1982)]; (2) an iterative scheme in which an initial temperature is guessed, based on which the mole fraction of all major species are calculated using their measured vibrational intensities. The mole fractions are then corrected using high–temperature correction factors to account for changes in the fraction of the Raman band falling in the exit slits provided for the respective photomultiplier tubes. The iteration process is repeated until the sum of the mole fractions is unity; and (3) Rayleigh scattering: Raman data on the major species were used to obtain the Rayleigh cross section of the mixture and thus provide temperature in an iterative manner. The last two methods agreed best, to within 10K on mean temperature and to within 50K on a shot–to–shot basis. Method (2), based on the sum of mole fractions of major species, is reported.

Initial measurements with the Raman system showed that there was significant laser–induced fluorescence (LIF) interference throughout the flame, as reported elsewhere [Masri and Dibble (1989), Dibble et al. (1990)]. The LIF was fairly broadband and contaminated all Raman channels, but was negligible in the Rayleigh channel. An additional difficulty was the crosstalk between CH_4 and other Raman channels, primarily O_2. For 488 nm excitation, the Raman interference in other major species was insignificant. To account for these two additional sources of contamination in the signals, the system and calibration procedures were modified. Additional photomultiplier tubes were installed in two Raman–free regions of the spectra to monitor the LIF on a shot–to–shot basis. These PMT's, termed F1 and F2, were located at 540nm (between O_2 and CO_2) and at 590nm (between CH_4 and H_2O), respectively. These two signals were found to correlate very well with each other and with all other Raman signals, so that the use of F1 was found to be sufficient to allow corrections in all other channels.

5

A calibration procedure was used to correct for the LIF, following the procedure of Dibble et al. (1990). A 38−mm−dia. honeycomb burner was built to provide laminar diffusion flames of 30%CH_4/70%CO. The flame was visibly sooty and yellow at the downstream end, and contained enough soot precursors and LIF. The calibration factors were obtained by iteration. First the raw data were used to calculate the temperature (from the sum of mole fractions) and mole fractions of major species. The contamination caused by fluorescence was particularly evident in the fuel−rich regions of the flame. The next step was to estimate correction factors for each of the major species based on the raw data, and to subtract a term equal to the product of the correction factor for species "i" and the value of the fluorescence signal measured in photomultiplier tube F1. The calculated temperature and mole fraction profiles were compared with predicted values. The process was iterated to convergence. Figure 2 shows the temperature and selected species so obtained. The temperature agrees fairly well with the predicted laminar flamelet calculations [Chen et al. (1989)] for an assumed stretch of 5/s; the calculations did not depend strongly on this assumed value. The corrections for N_2, O_2 and CH_4 are substantial, and the corrected species data again agreed with the laminar flame calculations, which are omitted for clarity. Calibration was repeated before and after each set of measurements.
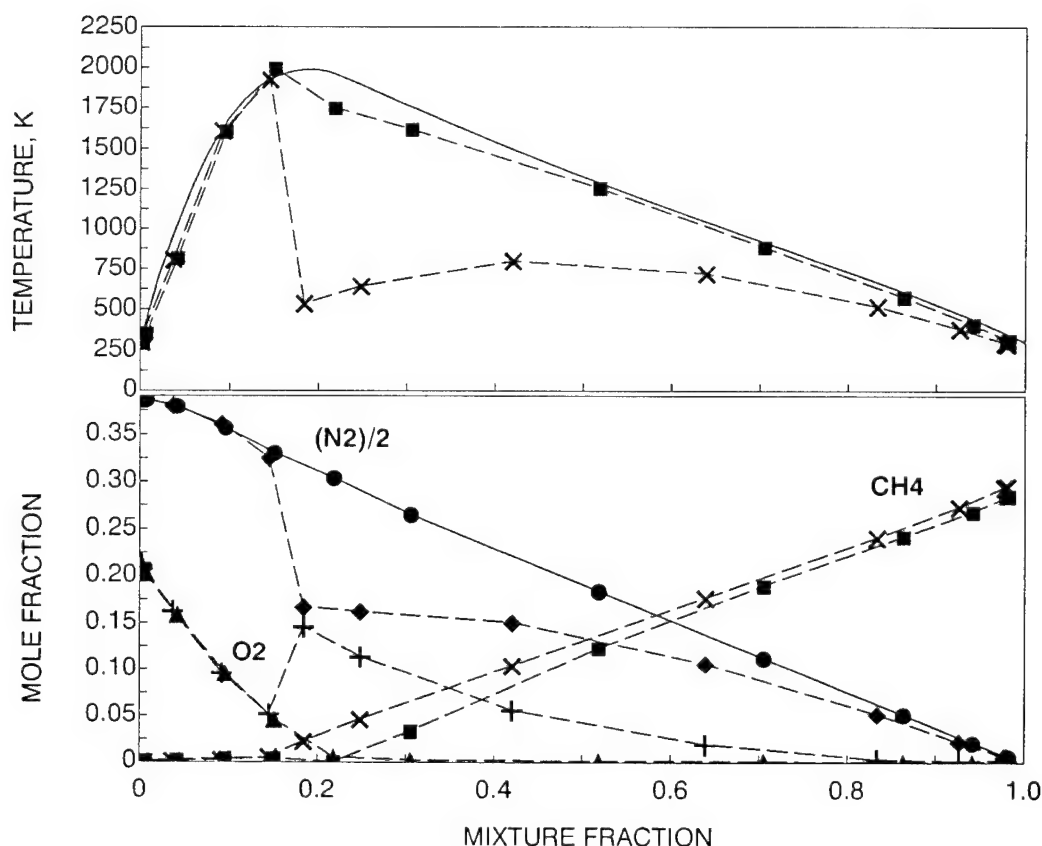

Figure 2. Raw and fluorescence−corrected Raman data. <u>Temperature.</u> "X"= raw data; "■" = corrected data; solid line = laminar flame calculation from Ref. 5. <u>Species.</u> raw data: "♦"= N_2, "+"= O_2 and "X"= CH_4; corrected data: "●"= N_2, "▲"= O_2, and "■"= CH_4.

Radial profiles of temperature and mole fractions of major species were measured at axial locations of x/d = 5, 10, 20, 30, 50 and 70 and along the centerline. Since not all these data can be discussed here, attention will be confined to the region of maximum turbulence, $10 \leq x/d \leq 20$.

To extend the pdf model from parabolic to elliptic flows, an iterative pdf/elliptic computational fluid dynamics (CFD) approach has been developed. The highly non−uniform CFD grid accounts for the disparate flow scales imposed by the jet and bluff body dimensions, with a second−order accurate numerical discretization scheme to eliminate numerical "diffusion" errors [Correa and Shyy (1987)].

The transport equation for the joint pdf $P(\underline{\Psi},\underline{V};x,t)$, which describes the joint probability of the fluid composition being the vector $\underline{\psi}$ and the fluid velocity being the vector $\underline{V}$ (at the position $\underline{x}$ and time t) is:

$$\varrho(\psi) \, \frac{\partial P}{\partial t} \; + \; \varrho(\psi) \, u_i \, \frac{\partial P}{\partial x_i} \quad + \quad [\, \varrho(\psi)g_j + \frac{\partial <p>}{\partial x_j} \,] \, \frac{\partial P}{\partial V_j} \quad + \quad \frac{\partial}{\partial \psi_\alpha} \, [\varrho(\psi)S_\alpha(\psi)P]$$

$$= \; \frac{\partial}{\partial V_j} \, [< \, - \frac{\partial \tau_{ij}}{\partial x_i} + \frac{\partial p'}{\partial x_j} \big|_{v,\psi} > P] \; + \; \frac{\partial}{\partial \psi_\alpha} \, [< \frac{\partial J_i^\alpha}{\partial x_i} \big|_{v,\psi} > P] \tag{1}$$

where $\underline{V}$ is the velocity field, the density ϱ is a function of the scalar variables denoted by the vector $\underline{\psi}$, and the reaction rate is $S_\alpha(\underline{\psi})$. The six terms describe, respectively, the evolution of the pdf; the transport of the pdf in physical space (x_i); the transport of the pdf in velocity space V_j by body forces and the mean pressure gradient; the transport of the pdf in composition space ψ_α by reaction $S_\alpha(\underline{\psi})$; the transport of the pdf in velocity space V_j by viscous stresses and the fluctuating pressure gradient; and the transport of the pdf in composition space by molecular fluxes. A one−point statistical description in terms of the joint pdf of the velocity and these scalars is sought. If the flow is statistically stationary, all one−point statistics depend only on the spatial coordinates. All one−point statistics are recovered from this pdf because the composition is a known function of the above scalars. The velocity−composition joint pdf evolution model relaxes many of the assumptions made in the standard closure, such as pdf shape, statistical independence of scalars, and gradient diffusion of scalars. Closure of the non−linear chemical source term or "turbulent fluxes" of scalars are given directly by the pdf.

Discussing specifically the case of methane, which is more complex than CO/H_2), the chemistry is described by the mixture fraction ξ, and the reactive scalars in the system. In the pdf transport equation, these become the independent variables denoted by $\underline{V}$, ψ, and ϕ_k (k=1,...4) respectively. The joint pdf evolves in this eight−dimensional velocity−composition space as well as in the two−dimensional x−r physical space.

Turbulent mixing of the scalars is modeled as a linear, deterministic relaxation to the local mean, sometimes called Interaction−by−Exchange−with−the−Mean (IEM) [Borghi (1988)]. The IEM model has been isolated and studied in detail in the Partially Stirred Reactor model, described next, and compared with other mixing models. Regarding the velocity term, the fluctuating component of acceleration (arising from the fluctuating pressure gradient and viscous forces) is modeled by the simplified Langevin model [Pope (1985), Pope (1990)]. The Seshadri−Peters (1990) 4−step reduced scheme is adopted for the kinetics. A look−up table of reaction rates, density and temperature is constructed on a non−uniform 20 x 10 x 10 x 10 x 10 grid.

The axisymmetric elliptic mean flow CFD model and the pdf model communicate with each other iteratively. On each time step, the fields of the mean velocity and the turbulence frequency, obtained from

the local turbulence kinetic energy (tke) and dissipation rate, are passed from the CFD model to the pdf model. A shift and a uniform stretching in $\underline{V}$ space are applied to the pdf so that the mean velocity and the tke of the two sub−models are in agreement. Thus the no−slip boundary condition is automatically satisfied at walls. Stochastic Lagrangian particle evolution, per the IEM model and the reduced scheme, occurs at the above frequency. The mean density field is passed back to the CFD model, and the two sub−models are iterated to convergence. The 75 x 60 cell, $\approx 10^5$ particle calculation was run until a statistical steady−state was achieved. For display purposes, lower moments such as the means were averaged over the last 200 time−steps of the pdf evolution, reducing statistical fluctuations in the results. Scatterplots were prepared from the calculations by saving several realizations of the pdf particle array after stochastic convergence, and then post−processing the more than 10^6 particles so obtained.

2.2 Comparison with Raman Data from Non−Premixed Bluff−Body Stabilized Flames

The following discussion focusses on the region of strongest turbulence ($10 \leqq x/d \leqq 20$), where the off−axis recirculation zone provides intense mixing at the edges of the jet.

Computed radial profiles of the mean and r.m.s. mixture fraction at x/d=20 compare well with the Raman data (Fig. 3). The measured radial profiles are shown in full, revealing the degree of symmetry, while the computed profiles are by assumption axisymmetric. The comparisons indicate that the calculated mixture fraction field is accurate enough to permit a meaningful evaluation of the reactive quantities. The mean temperature peaks in the recirculation zone with a maximum of less than 1000K, a result of the strong turbulence. Computations and data agree quite well (Fig. 4), although the temperature is underpredicted by almost 250K along the centerline. The mean major species profiles also agree quite well (Fig. 5). The mean O_2 is depleted in the wake of the bluff−body but coexists with mean CH_4, a consequence of finite−rate chemistry. The O_2 returns to ambient levels at the edge of the bluff−body ($r \cong 0.02$ m). The model predicts more mean O_2 than measured at the centerline, which is consistent with underprediction of the mean temperature in Fig. 4.

Scatterplots provide an instructive format in which to study turbulence−chemistry interactions, and best utilize the power of the time− and (not quite) space−resolved Raman spectroscopy and the pdf model. The measured temperature−mixture fraction scatterplot using all data from x/d=10 and x/d=20 is shown in Fig. 6 (a), along with the calculated laminar flame profile for a stretch of 5/s [Chen et al. (1988)]. Unlike in the CO/H_2 flame studied previously, bimodality is clearly evident. A significant number of points has mixture fraction values close to stoichiometric but temperatures which manifest localized extinction, while other points are clustered along the line of strained flamelet temperatures. The physical picture that emerges from the scatterplots is that of a recirculation zone (which anchors the turbulent flame), connected to a jet−like region by a narrow neck of high shear with a significant amount of local extinction.

The corresponding calculated scatterplot (Fig. 6 (b)) is similar, although the predicted points exhibit a greater trend towards extinction. On a related note, stochastic calculations of lean methane−air combustion in a Partially Stirred Reactor [12] showed that the parent starting scheme used to develop the 4−step model agreed with a 77−step scheme reasonably well when the mean temperatures were above 1500K, but prematurely predicted blowout relative to the 77−step scheme. This behavior is similar to the overprediction toward extinction in the present study.
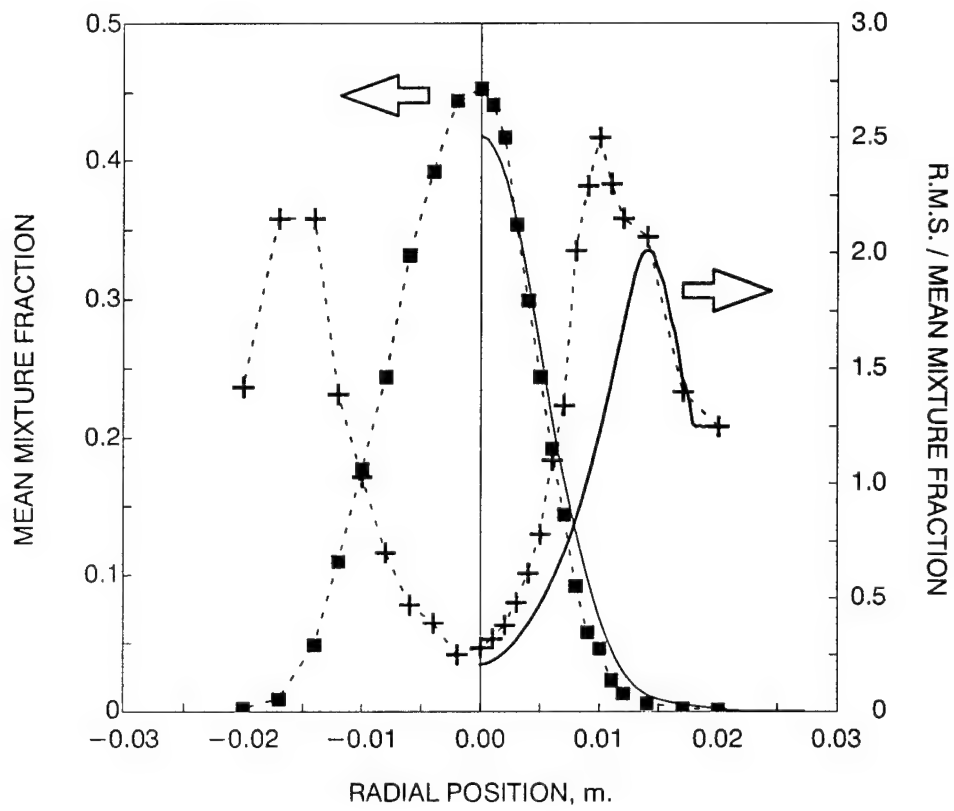
8

Figure 3. Comparison of mean and RMS mixture fraction profiles at x/d=20. Raman data: "■" and "+"; Calculations: solid lines.
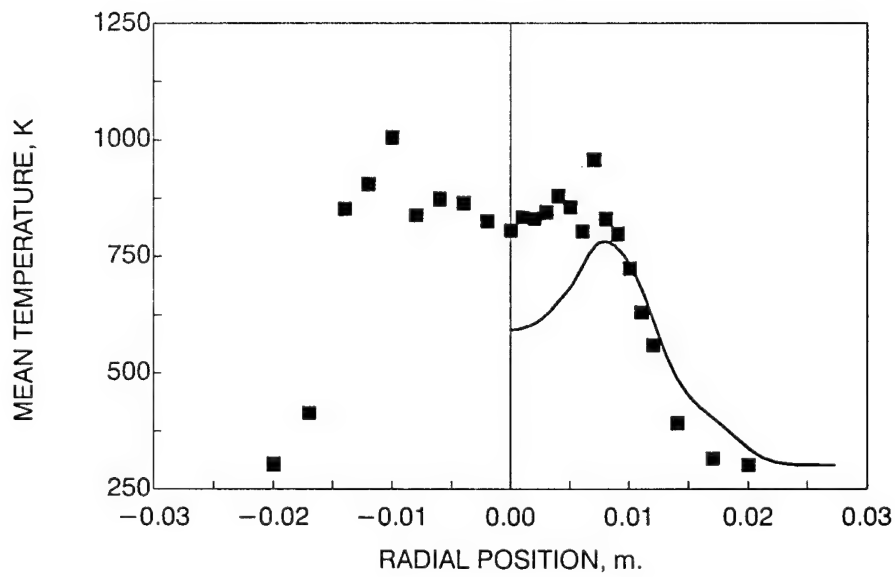

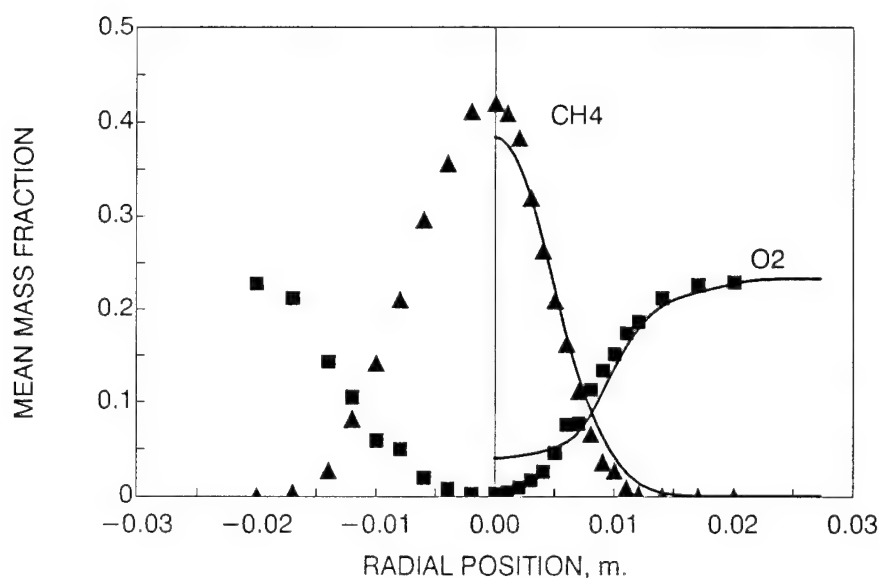Figure 4. Comparison of mean temperature profiles at x/d=20.

Figure 5. Comparison of mean CH_4 and O_2 profiles at x/d=20.

The coexistence of fuel and oxygen is again apparent in Y_{CH4}–Y_{O2} scatterplots (not shown) from both the data and the model. The measured and calculated scatterpoints at x/d=20, both of T–ξ and Y_{CH4}–Y_{O2}, were closer to the chemically "frozen" line than those at x/d=10, in accordance with Raman data and with visual observations of the flame.

The calculated CO scatterplots have maxima of 3% (inset: Figure 7) whereas the data peak at about 10% (Figure 7), well above the flamelet maxima. Similar 10% levels were measured in Masri et al. (1992) bluff body flame and in pilot–stabilized flames [Chen et al. (1989)], and 2–3% peaks were predicted in the latter using the 4–step scheme within a (scalar) pdf/Reynolds stress model. Hence, this discrepancy on CO maxima has appeared in diverse circumstances (but always in combustion gases that are near local extinction). There are many potential contributors, including: (i) the assumption of a steady state for the radicals in the 4–step mechanism; (ii) the errors in Raman–based CO and CO_2 data, as discussed above, and as seen by direct comparison with predicted mean CO and CO_2 profiles in the CO/H_2 bluff body flame of Correa and Pope (1992); and (iii) neglect of phenomena such as unsteady flamelets or micromixed gases (perfectly stirred reactors), which have been shown to lead to high CO [Mauβ et al. (1990), Chen and Dibble (1991)]. In intense turbulence, however, the microscale may be better simulated by the PaSR – described in the next section – since it is the degenerate form of the pdf equation for spatially homogeneous systems. For example, at 30 atm the PaSR indicates that approximately 2% peak CO levels are encountered until the fuel is pyrolyzed and CO oxidation can commence [Correa (1994)]. It seems clear that CO is an important clue to the microstructure of highly turbulent combusting gases, and that accurate measurements will be critical.

10
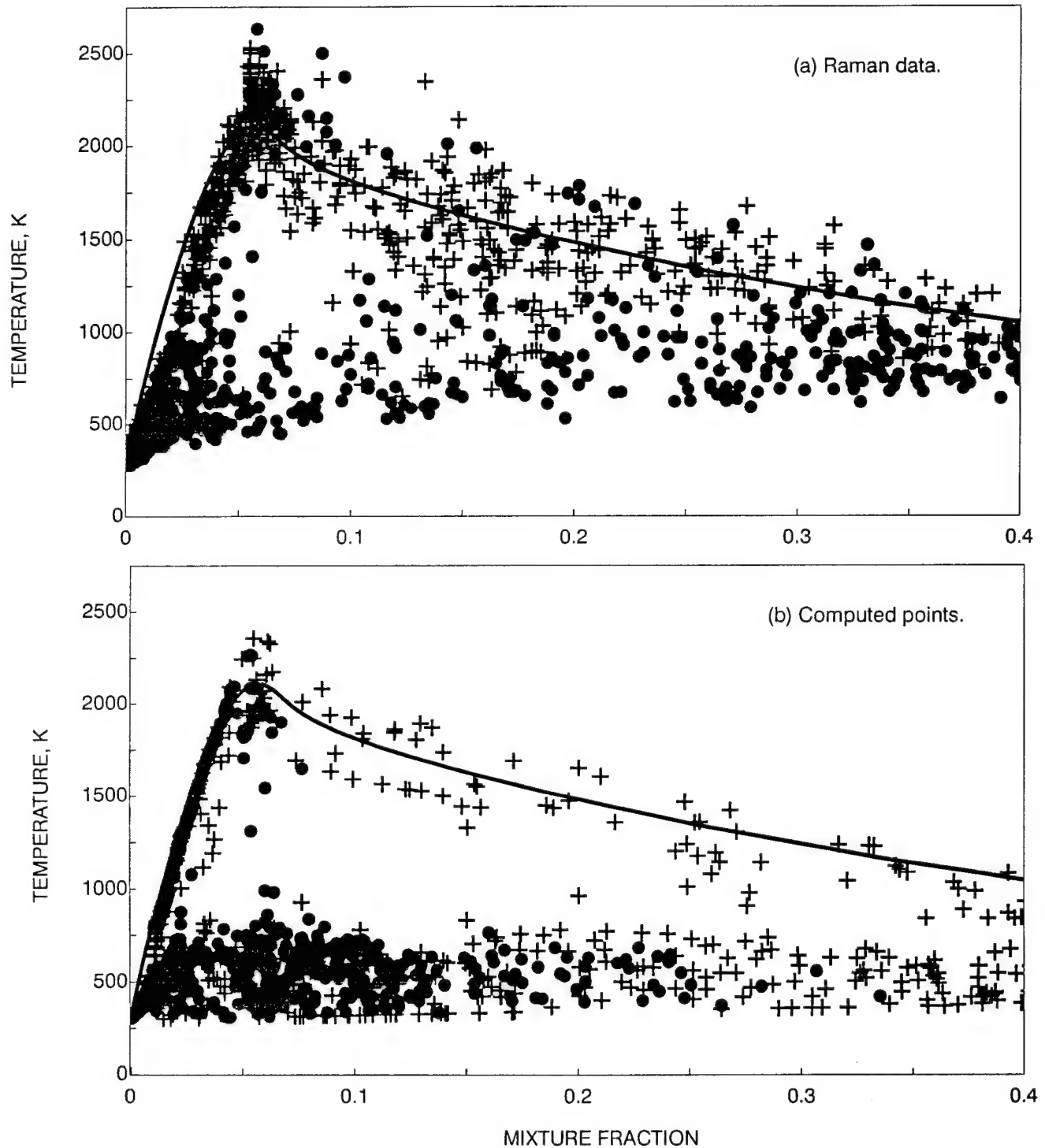
Figure 6. Temperature−mixture fraction scatterplot at x/d=10 (plus symbols) and x/d=20 (solid symbols). Solid line is laminar flame calculation, from Chen et al. (1989).

11
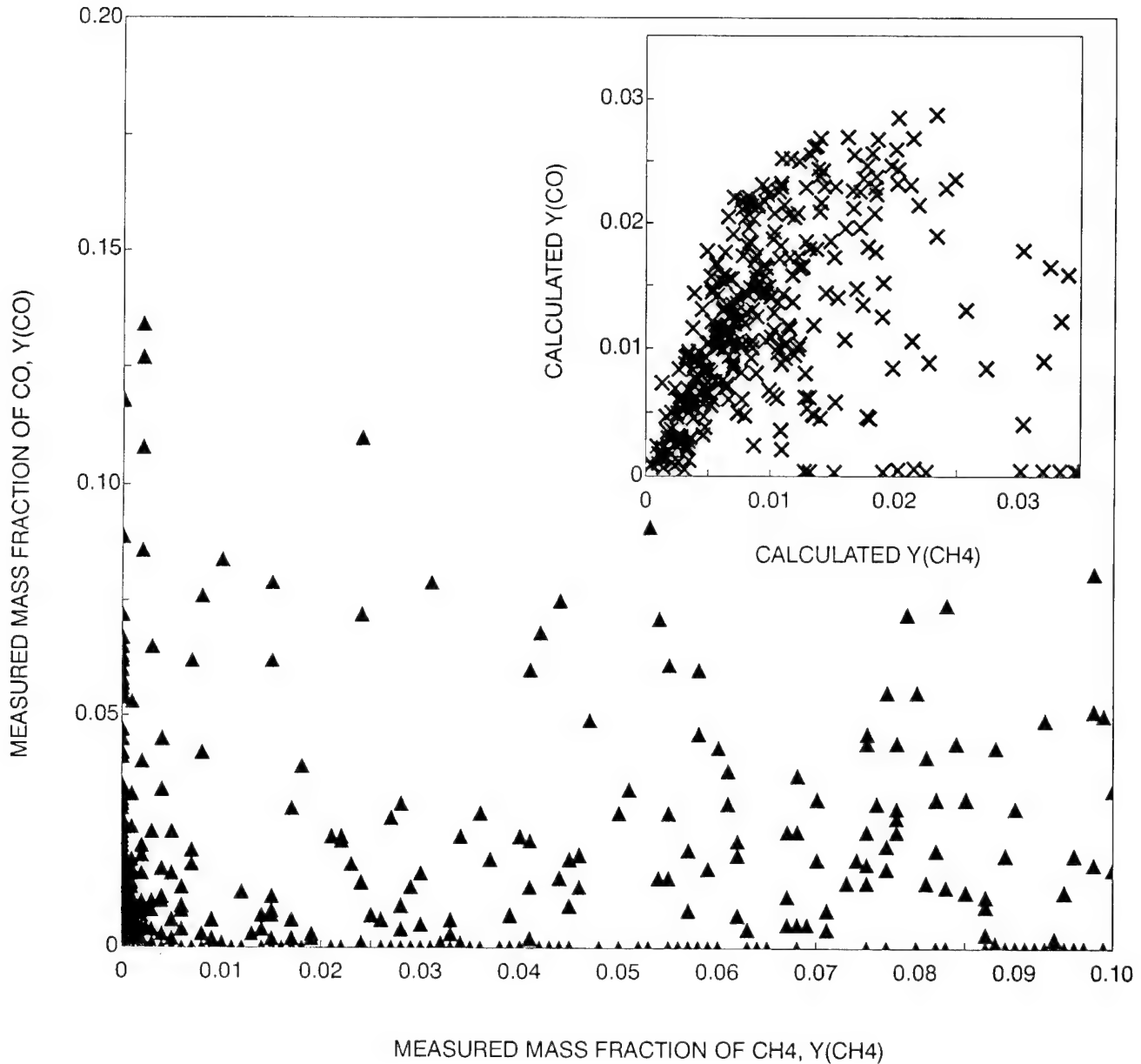
Figure 7. CO−methane scatterplot at x/d=10 and x/d=20.

Because the joint pdf contains the velocity components of each particle, the scalar fluxes can be examined. Figure 8 shows the computed radial transport $\overline{v'\xi'}$ of the mixture fraction at x/d=20, calculated by summing over particles in twenty radial bins. Also shown is the gradient diffusion flux $-(\mu_t/\overline{\varrho})\,\partial\overline{\xi}/\partial r$, the latter computed from the mean fields; μ_t is the turbulent viscosity computed from the k−ε equations. Both fluxes were calculated a *posteriori*, since they were not needed for the main computation. Figure 8 shows that in the presence of the strong radial gradient $\partial\overline{\xi}/\partial r$, (radial) transport of the mixture fraction is consistent with the notion of gradient diffusion, i.e., there is no counter−gradient diffusion. The magnitude of $\overline{v'\xi'}$ is, however, much greater than that of $-(\mu_t/\overline{\varrho})\,\partial\overline{\xi}/\partial r$. The indicated "turbulent Schmidt number" is about 0.4.

12
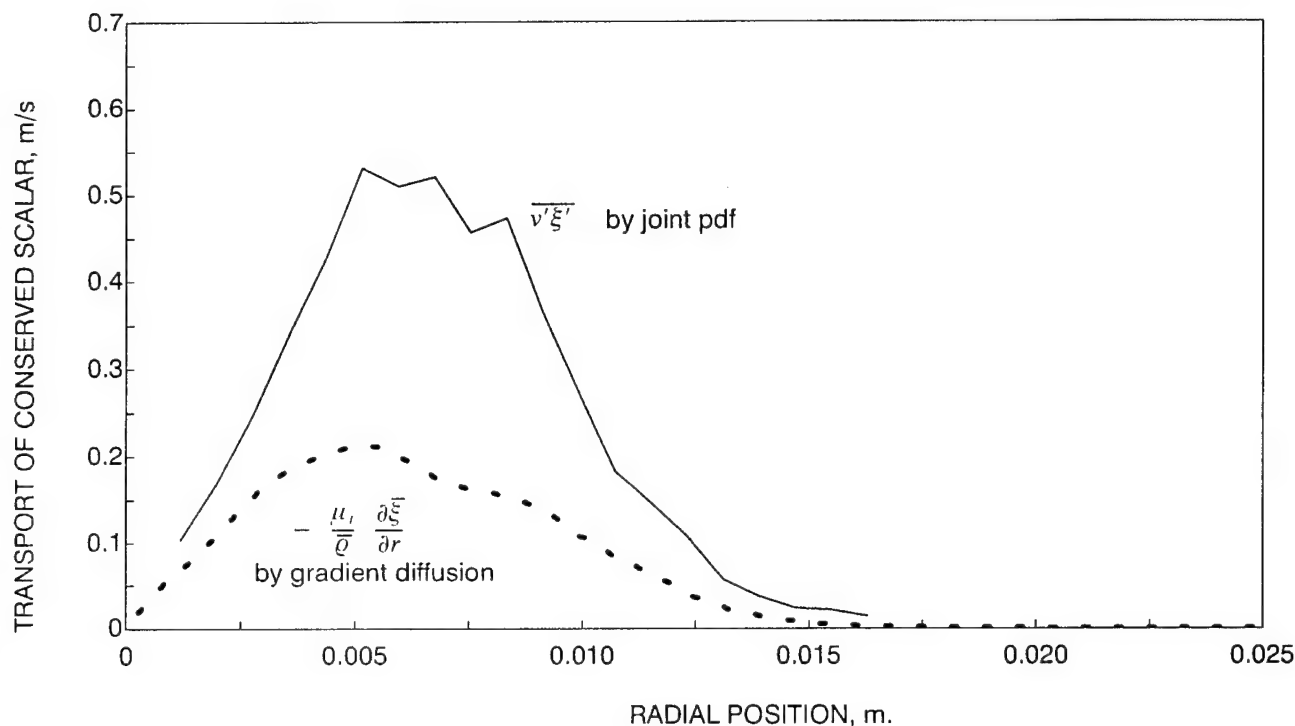
Figure 8. Radial flux of conserved scalar at x/d=20.

The study demonstrates several points:

1. The bluff body burner provides a strongly turbulent field leading to localized extinction, without the need for a pilot flame. Thus the two−stream nature of the problem is preserved, unlike many piloted jet flame studies where the composition or the excess enthalpy of the pilot flame can cause modeling difficulties. The present recirculation−stabilized flame is also much closer to practical burners.

2. By correcting for fluorescence, Raman measurements can be made in bluff−body CH_4−air flames; however, the errors in certain species (e.g., CO and CO_2) may be so large that models should not be changed on the basis of such data alone.

3. Given the similarity in scatterplots, it is clear that the pointwise structure of the above bluff body flame and the piloted jet flame are quite similar. A greater degree of local extinction is measured here.

4. The limitations of pdf shape assumption, statistical independence of scalars, and gradient diffusion, are removed in this model. The consequences can be seen in joint scatterplots and in convective fluxes.

The acquisition of Raman data and the 3−velocity/5−scalar joint pdf calculation in this bluff body methane flame takes each "discipline" to the limits of the present state of the art. Any significant further progress will require improvements in major species measurements, complementary velocity and minor species measurements, and parallel computers. Reduced chemistry schemes that relax steady state assumptions (and are likely to require additional scalars) will have to be developed and assessed in simpler contexts.

13

2.3 The Need for an Improved Prototype of Highly–Intense Turbulent Combustion

The laminar flame speed depends on the fuel–air equivalence ratio "Φ" and the pressure "p," and has been computed for the methane–air system by several research groups with reasonable agreement [Smooke and Giovangigli (1990), Seshadri and Peters (1990)]. Taking the inlet temperature T_{in} to be 300K in the base case, the flame speed drops from about 40 cm/s in the stoichiometric atmospheric–pressure case to about 10 cm/s in lean atmospheric–pressure flames, and similarly in stoichiometric high–pressure flames. The flame speed would decrease further with strain. On the other hand, recent calculations by Smooke (1993) indicate that the flame speed rises with inlet temperature; this behavior is relevant to high–pressure combustion because the fuel–air premixture is preheated by the (usually nearly adiabatic) compression process. It is clear, however, that the laminar methane–air flame speed is less than 2 m/s under conditions T_{in} < 700K and Φ < 0.6. The latter are typical of, for example, a low–emissions lean premixed gas–turbine combustor operating at a pressure of 15 standard atmospheres in the burner.

Next, consider the above flame speed relative to the turbulence intensity. Taking a typical combustor mean flow velocity of 100 m/s and a typical turbulence intensity of 10%, the turbulent velocity fluctuations are on the order of 10 m/s, i.e., on the order of ten times the laminar flame speed. The topology of the laminar flame will not survive in turbulence of such intensity. This argument can also be advanced by comparing the time–scales of all relevant mixing processes (given by the turbulence spectrum) with the time–scales of all relevant chemical reactions. The ratios are called the Damkohler numbers: values much less than unity suggest behavior approaching stirred reactors [Bilger (1988)], while values much larger than unity are necessary for the flamelet model to hold [Peters (1986)]. It can easily be shown that in real systems the Damkohler numbers span several orders of magnitude about unity, so flamelet behavior does not exist for all the reaction/mixing process pairs that are operative [Correa (1992)].

From the above, it may be concluded that an intense combustion process should not be viewed as the motion of a high–speed flamefront. Another viewpoint is that of chemical reactions in a highly–loaded reactor devoid of spatial features. The "linear eddy" model provides a one–dimensional framework spanning these two extremes [Kerstein (1991)]. Transport by turbulent "eddies" is accounted for by random rearrangement of the scalar field(s) along a line, at a rate and with (a distribution of) length scales in accordance with fundamental scaling rules taken from the theory of homogeneous turbulence. In between these folding events, molecular diffusion (and chemical reactions) can occur along the line. As the turbulence amplitude and frequency increase, the relevance of reaction–diffusion interfaces (flamefronts) decreases. Ultimately, the velocity field and the spatial structure become less important and a stirred reactor description would be more appropriate.

2.4 Development of the Partially–Stirred Reactor Model

A stochastic model operating in N_s–dimensional composition space has been developed for the latter class of spatially homogeneous, but not mixed, reacting flows. The model, called the Partially Stirred Reactor or "PaSR," is described next.

The PaSR model has two applications:
(i) as the closure model for the multi–dimensional joint pdf model. In this application, simplified chemical schemes are typically used. An example is the combined CFD (Computational Fluid Dynamics) and joint pdf calculation of a bluff–body (recirculation) stabilized CH_4 flame, which used five scalar variables to de-

scribe the chemistry; and
(ii) for standalone calculations of the intensely turbulent but not perfectly stirred regime, decribed in the following sections.

The PaSR was developed in this program during this reporting period [Correa (1993 a)]. The governing equations may be derived from the joint pdf equation [Pope (1990)] by specialization to homogeneous but unmixed flow, obtaining:

$$\varrho(\Psi) \frac{\partial P}{\partial t} + \frac{\partial[\varrho(\Psi)S_\alpha(\Psi)P]}{\partial \psi_\alpha} = \frac{\partial[<\frac{\partial J_i^\alpha}{\partial x_i}|_{v,\Psi} > P]}{\partial \psi_\alpha} \tag{2}$$

Physically speaking, reactants flow into a "box" whose contents — reactants, products and intermediates — are mixed by turbulence of a prescribed frequency (Fig. 9). A steady state of "unmixedness" is maintained by the compositional difference between the inlet stream and the contents of the reactor. The pdf $P(Y_k)$ of mass fractions Y_k of species in the reactor is represented by the N_p- particle ensemble

$$Y_k^{(1)}, Y_k^{(2)}, \ldots\ldots Y_k^{(n)}, \ldots.. Y_k^{(N_p)}; \qquad k = 1, \ldots.N_s$$

where $N_s \equiv$ number of species and $N_p \equiv$ number of particles. Scalar mixing is accounted for by the "Interaction—by—Exchange—with—the—Mean" (IEM) submodel [Borghi (1988)]. The particle equations are

$$\frac{dY_k^{(n)}}{dt} = -C_\phi \omega(Y_k^{(n)} - \overline{Y}_k) + w_k^{(n)} \frac{M_k}{\varrho^{(n)}}; \qquad k = 1, \ldots.N_s \tag{3a}$$

where ω is the mixing frequency in the IEM model, $w_k^{(n)}$ is the molar production rate of species "k" per unit volume for the nth particle, M_k is the molecular weight of species "k" and $\varrho^{(n)}$ is the density of the nth particle. Equation 3 (a) is solved as shown, without fractional steps; therefore, mixing and chemistry are accounted for simultaneously. The corresponding equation for particle temperature is

$$\overline{C}_p \frac{dT^{(n)}}{dt} = \frac{dH^{(n)}}{dt} - \sum_{n=1}^{N_s} h_k \frac{dY_k^{(n)}}{dt} \tag{3b}$$

where $H^{(n)}$ is the total enthalpy of particle "n." Hence, the PaSR is described by a coupled system of $(N_s + 1) \times N_p$ first—order stiff ordinary differential equations (o.d.e.'s).

The mass flow rate m into the PaSR is discretized into N_{in} particles per global time step (Fig. 9). Particles, selected randomly from the ensemble, flow out at the same mass flow rate. Particles in the ensemble evolve according to Eqs. 3. The integration is continued until a stochastic steady state is achieved. Scatterplots, pdf's, and correlations of interest can be obtained from the steady state ensemble. The global residence time can be computed as $\tau \equiv \overline{\varrho}V/m$, where $\overline{\varrho}$ is the mean density (obtained by appropriately summing over particle masses and volumes) and V is the reactor volume; τ also converges.
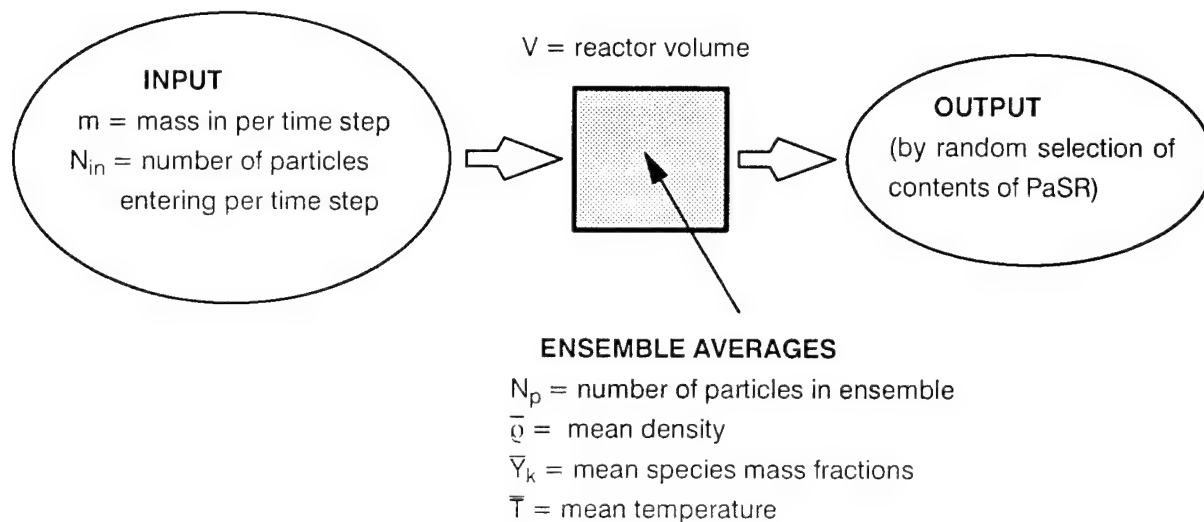
15

Figure 9. The PaSR model. The PaSR may be viewed as a single computational cell in the multi−dimensional CFD/pdf model and hence previews the eventual capability of the latter.

2.5 Parallelization

Expensive numerical integration techniques, such as the Gear method, are required because of the stiffness of the o.d.e.'s when complex kinetics are considered. Therefore the PaSR model entails considerable computational cost. Further examination indicates that solving the systems of ordinary differential equations for each of the particles (i.e., Eqs. 2 and 3) takes up almost all the computational time. As a prelude to the present study, the PaSR algorithm was evaluated on parallel computers with a view to reduction of run time. The term "parallel" refers to a computer architecture in which multiple linked processors work in parallel on different particles, according to techniques described below. The IEM model lends itself extremely well to parallel computing because the terms in the $(N_s+1) \times N_p$ particle equations contain properties of only (i) the present particle and (ii) the ensemble; it is not necessary for any one particle to "know" about other particles individually, but only indirectly through the interaction with the mean calculated from the previous time step. As a result, all particles can be advanced in parallel within a time step. Individual particles or groups of particles can be computed on different processors. Parallelization of this sort is referred to as particle partitioning, since each processor operates on a sub−ensemble of particles. At the end of the time step, communication between the processors is required to allow the mean properties to be computed for use in the next time step.

The approach taken was to parallelize the PaSR algorithm in as simple a fashion as possible. Since the solution of the particle equations takes up almost all of the time, only that portion of the code was parallelized. The inflow/outflow particle management, computation of means, and other overhead functions were performed redundantly on each processor. The storage requirements of the code are modest enough to allow the global data to be replicated on each processor. The parallel implementation is targeted at distributed memory MIMD (multiple instruction, multiple data set) computers such as the Intel iPSC/860 and Intel

Delta. The code was written in FORTRAN 77 with Intel's message passing calls to support the required inter-processor communication.

Particles can be allocated to processors either statically or dynamically. In a static allocation, the number of particles in the simulation is divided by the number of available processors as evenly as possible. In a dynamic allocation, the particles are dealt dynamically to processors by some control processor. As a processor finishes the calculations for a particular particle, it is assigned the job of solving the equations for the next particle. Note that dynamic allocation, in which different processors perform different tasks, requires a MIMD architecture. SIMD computers (SIMD stands for single instruction, multiple data set) in which each processor does essentially the same thing at the same time, are only suitable for static allocation.

An important characteristic of the algorithm considered here is that the solution time varies significantly from particle to particle. The ordinary differential equations for each particle are solved by an explicit time−marching Gear's method which adaptively adjusts the step size to maintain stability. The solution times vary because of the varying stiffness of the equations for different particles. As a result, static allocation of equal numbers of particles to each processor leads to poor load balance. To illustrate this in specific terms, we repeat combustion of CO/H_2 fuel as represented by a scheme of 18 species and 43 reactions [Correa (1993)] with parameters set such that all runs involved 360 global time steps and 762 particles. Figure 10 shows typical results of static allocation with 10, 20, 30, and 40 particles assigned per processor. Notice that the load balance does not improve substantially as the number of particles per processor is increased, as might be expected from the law of averages. In fact, the imbalance with 30 particles per processor is seen to be significantly worse than with either 10 or 20 particles per processor.

Dynamic allocation through the use of a "manager−worker" scheme is found to lead to significantly better load balance, and to higher parallel efficiencies (i.e., speedup relative to a single processor normalized by the number of processors). One processor is designated the "manager," and given the job of dealing out the particles to the other processors ("workers"). As a worker processor finishes calculating the time step for its particle, it signals the manager that it is available to perform another calculation. In this manner, a processor that is assigned particles that can be solved quickly will calculate more particles, while a processor that is assigned particles that take a long time to solve will calculate fewer particles. Figure 11 shows the number of particles dynamically assigned to each processor for the same test case considered in Fig. 10. The number of particles assigned is not at all constant, but is seen to vary significantly from processor to processor. When the average number of particles per processor exceeds ten or so, dynamic allocation smooths out the load balance well (Fig. 12). The maximum time required by any processor is also seen to be significantly smaller with dynamic allocation than the maximum time required by any processor with static allocation, as comparison of Figs. 10 and 12 shows. The comparison is striking in the case with 480 particles, where dynamic allocation reduces the maximum time from 22.5 seconds to about 19 seconds.

For dynamic allocation to be efficient, each processor must have equal access to the data needed to perform the requested calculation. The algorithm under consideration here requires relatively little total storage, allowing the global data to be replicated on each processor and hence making dynamic allocation feasible. One drawback of the Intel iPSC/860 is that only a single process can run on each processor. As a result, the manager processor sits idle much of the time while the worker processors perform their computations, because it is not possible to start an additional worker process on the manager processor. A practical consequence of this is that on a computer with N_p processors, only N_p-1 processors are solving the par-

ticle equations. This is clearly more of a drawback on small computers than on large massively parallel machines. The improved load balancing achieved by dynamic allocation more than offsets this disadvantage on the larger machines. Dynamic allocation is superior to static allocation when six or more processors are used. The falloff in the improvement achieved on the Delta as the number of processors is increased is a result of the number of particles per processor becoming small (here, < 10), which reduces the effectiveness of dynamic allocation in smoothing out the load imbalance between processors as discussed above.

Another important consideration in the parallelization of Monte−Carlo algorithms is the generation of random numbers on a parallel computer versus a serial computer. One of the objectives in parallelizing the PaSR model was to ensure that the both the convergence path and the final solution were independent of the number of processors used. This requires that the same particles are removed from the reactor as new particles are introduced on each and every processor at every stage of the calculation. This was accomplished in an almost trivial manner here by redundantly performing the particle removal on each processor, and by starting the same random number generator on each processor with the same seed so that identical sequences of random numbers were generated. Had this portion of the calculation also been performed in parallel, special care would have been required to guarantee identical results.

The calculation of the mean at the end of the time step requires global communication between the processors since each processor only updates the solution at the time step of interest for a sub−ensemble of particles. There are two different ways of calculating the mean that can be used. One method is to have each processor compute the sum of all of the properties on its sub−ensemble, and then globally exchange the sums. Another method is to have each processor perform a global shuffle of each of the columns of the solution vector it computed with each of the other processors, so that each processor ultimately reconstructs the entire solution vector. At this point, the mean properties can all be computed redundantly by each processor, using the same code as in the serial implementation. The first method is more computationally efficient because the computation of the means is done partially in parallel, and because less data must be communicated. However, the method suffers the potential drawback of roundoff error because the sums on the different processors are not all computed in the same order and the results may be slightly different. The second method requires more comunication, but ensures identical results on each processor.

Timing results indicate that the parallel inefficiency observed is caused primarily by load imbalance, and that the time required to globally communicate the results and compute the means is insignificant. Consequently, either method of computing the means appears adequate for this application. The second method was used here because it required fewer modifications to the code and ensured identical results.

To verify the parallelization and demonstrate the speedup, a CO/H_2 scheme per Table I was calculated on (i) four serial computers: a Sun Sparcstation 1, a Convex C210, a Cray Y−MP, and a Cray Y−MP C90 (hereafter called a Cray C90), and (ii) two parallel computers: a hypercube−based 16−node Intel iPSC/860, and the mesh−based 512−node Intel Touchstone Delta prototype. The Cray runs were made with the original version of the code, and repeated with a version optimized in a machine−specific manner.

Examining the run times (cpu time), the PaSR code on the 16−node Intel hypercube was found to run about 1.4 times faster than on the Cray C90 and about 17.1 times faster than on the CONVEX. The run on 256 processors of the Intel Delta took 26 minutes. This result was 17.7 times faster than the run of the original code on the C90, and 10.7 times faster than the run of the modified code on the C90. Although a single

18

processor of the Intel computers is about a factor of ten slower than the Cray C90, the PaSR algorithm does not "vectorize" well and therefore the principal feature of the latter machine cannot be exploited. It should be mentioned that this is not characteristic of all classes of equations; for example, conventional computational fluid dynamics (CFD) codes are significantly accelerated on vector computers.

Summarizing the results of parallelization, Fig. 13 indicates that the rate of computation ("Mflop" ≡ millions of floating point operations per second) is linear in the number of processors, up to the level of 64 processors on the Intel machines. A yield of approximately 4 Mflop/processor is obtained on the iPSC/860 processors in this range. The speedup is less than linear as the number of particles per processor becomes less than 10, because then the dynamic allocation is less able to achieve good load−balancing. The initial conditions on the particle in each global time step greatly affect the stiffness of the governing o.d.e.'s, and so the computational time. With a large number of particles per processor, the total computational load becomes similar for each processor; at the other extreme, the load can be very disparate. In this limit, most of the processors may have to "wait" for the few that are integrating the stiffest sub−sets of the equations. On the other hand, had about 5,000 particles been used in Fig. 13 (note that 115,000 particles were used in the combined CFD/pdf transport calculation of Section 2.2, albeit with simple chemistry) a rate of about 2 GFlops (4 Mflops x 512 processors of the Delta machine) could have been attained.

It is clear that distributed memory MIMD parallel architectures are well suited to the particle−tracking PaSR algorithm. This remains true so long as the turbulence model does not require continuous communication between "particles." Thus, the IEM model is preferable to pair−exchange models on the parallel computers.

2.6 CH$_4$/Air System

We have used the PaSR model to study a 27−species/77−reaction methane oxidation scheme per Table II [Correa and Braaten (1993)]. The calculation involved 600 to 700 particles and therefore ≈20,000 o.d.e.'s. Figure 14 shows typical results for a 30 atm, 1200K (inlet) premixed methane−air system. Figure 14 (a) shows the convergence of ensemble−mean Y_{CO} to a stochastic steady−state; the degree of turbulence in the time−histories of species is greatest for CO (among major species) as blowout is approached. Figure 14(b) shows that the PaSR solutions properly meet the limits imposed by PSR and PFR models; note that with this choice of inlet conditions, reactor volume and mass flow (such that the residence time τ turns out to be approximately 2 ms), the flame blows out in the low frequency limit. Figure 14 (c) shows that the "skeletal" mechanism (used by Seshadri and Peters (1990) as the basis for the 4−step reduced scheme in laminar flames) cannot reproduce the full scheme's results at low frequency, where ignition chemistry becomes important. Figure 14 (d) shows a typical scatterplot , here for NO_x although any one of the 27 species or temperature could have been shown. The scatterplots can be used to derive pdf's, correlations, rms's, and other quantities.

We have only briefly summarized the development and some key conclusions of the PaSR model. Many more results and sensitivity analyses are given in Correa and Braaten (1993), Correa (1993), and Correa (1994 a). The PaSR model has also been adopted as an investigative tool by other researchers, e.g, at the University of Sydney and at UC−Berkeley.

Table I. Kinetic Mechanism Used for CO/H_2–Air Combustion.

(Forward rate constant $k_f = A\, T^b\, e^{-E/RT}$, moles–cm–s–K; E units: cal/mole)

No.	Reaction	A	b	E
1.	CO+O+M=CO2+M	3.20E+13	0.0	−4200.0
2.	CO+OH=CO2+H	1.51E+07	1.3	−758.0
3.	CO+O2=CO2+O	1.60E+13	0.0	41000.0
4.	HO2+CO=CO2+OH	5.80E+13	0.0	22934.0
5.	H2+O2=2OH	1.70E+13	0.0	47780.0
6.	OH+H2=H2O+H	1.17E+09	1.3	3626.0
7.	H+O2=OH+O	2.00E+14	0.0	16800.0
8.	O+H2=OH+H	1.80E+10	1.0	8826.0
9.	H+O2+M=HO2+M	2.10E+18	−1.0	0.0

H2O enhanced by 21.0, CO2 enhanced by 5.0, H2 enhanced by 3.3,

CO enhanced by 2.0, O2 enhanced by 0.0, N2 enhanced by 0.0

No.	Reaction	A	b	E
10.	H+O2+O2=HO2+O2	6.70E+19	−1.4	0.0
11.	H+O2+N2=HO2+N2	6.70E+19	−1.4	0.0
12.	OH+HO2=H2O+O2	5.00E+13	0.0	1000.0
13.	H+HO2=2OH	2.50E+14	0.0	1900.0
14.	O+HO2=O2+OH	4.80E+13	0.0	1000.0
15.	2OH=O+H2O	6.00E+08	1.3	0.0
16.	H2+M=H+H+M	2.23E+12	0.5	92600.0

H2O Enhanced by 6.0, H enhanced by 2.0, H2 enhanced by 3.0

No.	Reaction	A	b	E
17.	O2+M=O+O+M	1.85E+11	0.5	95560.0
18.	H+OH+M=H2O+M	7.50E+23	−2.6	0.0

H2O enhanced by 21.0

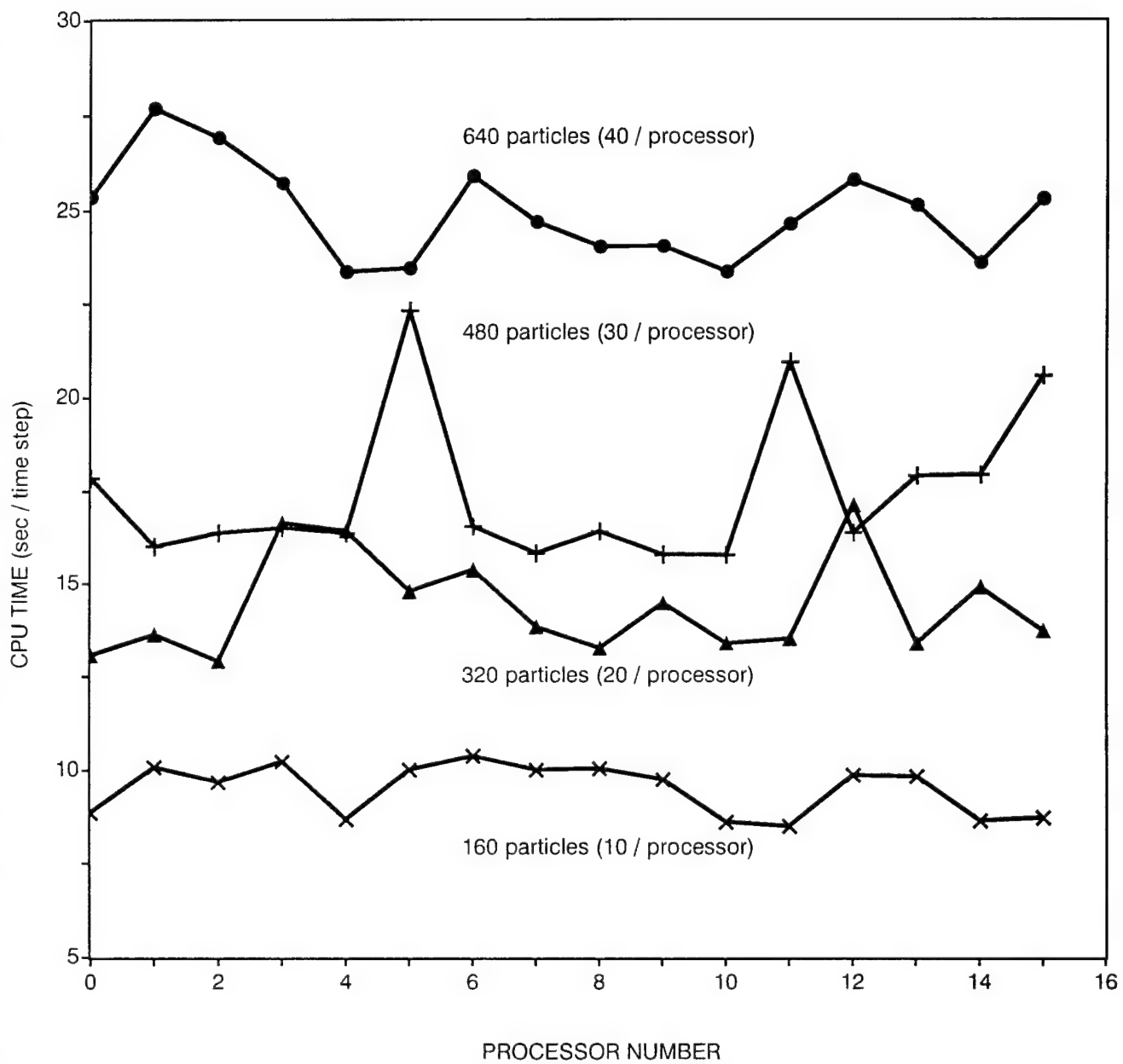| No.	Reaction	A	b	E
19.	H+HO2=H2+O2	2.50E+13	0.0	700.0
20.	HO2+HO2=H2O2+O2	2.00E+12	0.0	0.0
21.	H2O2+M=OH+OH+M	1.30E+17	0.0	45500.0
22.	H2O2+H=HO2+H2	1.60E+12	0.0	3800.0
23.	H2O2+OH=H2O+HO2	1.00E+13	0.0	1800.0

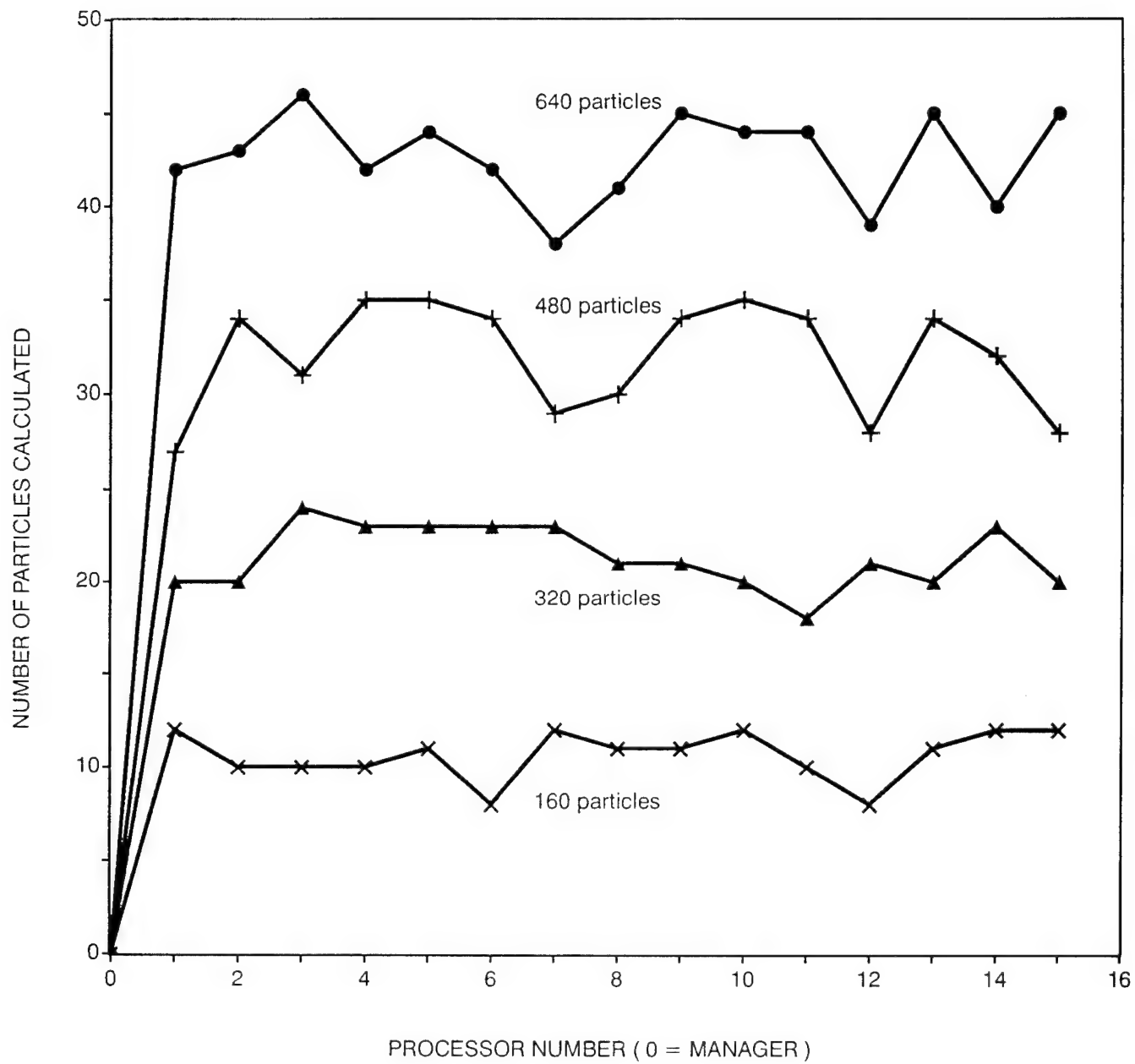Figure 10. Load Imbalance resulting from static allocation of particles to processors.

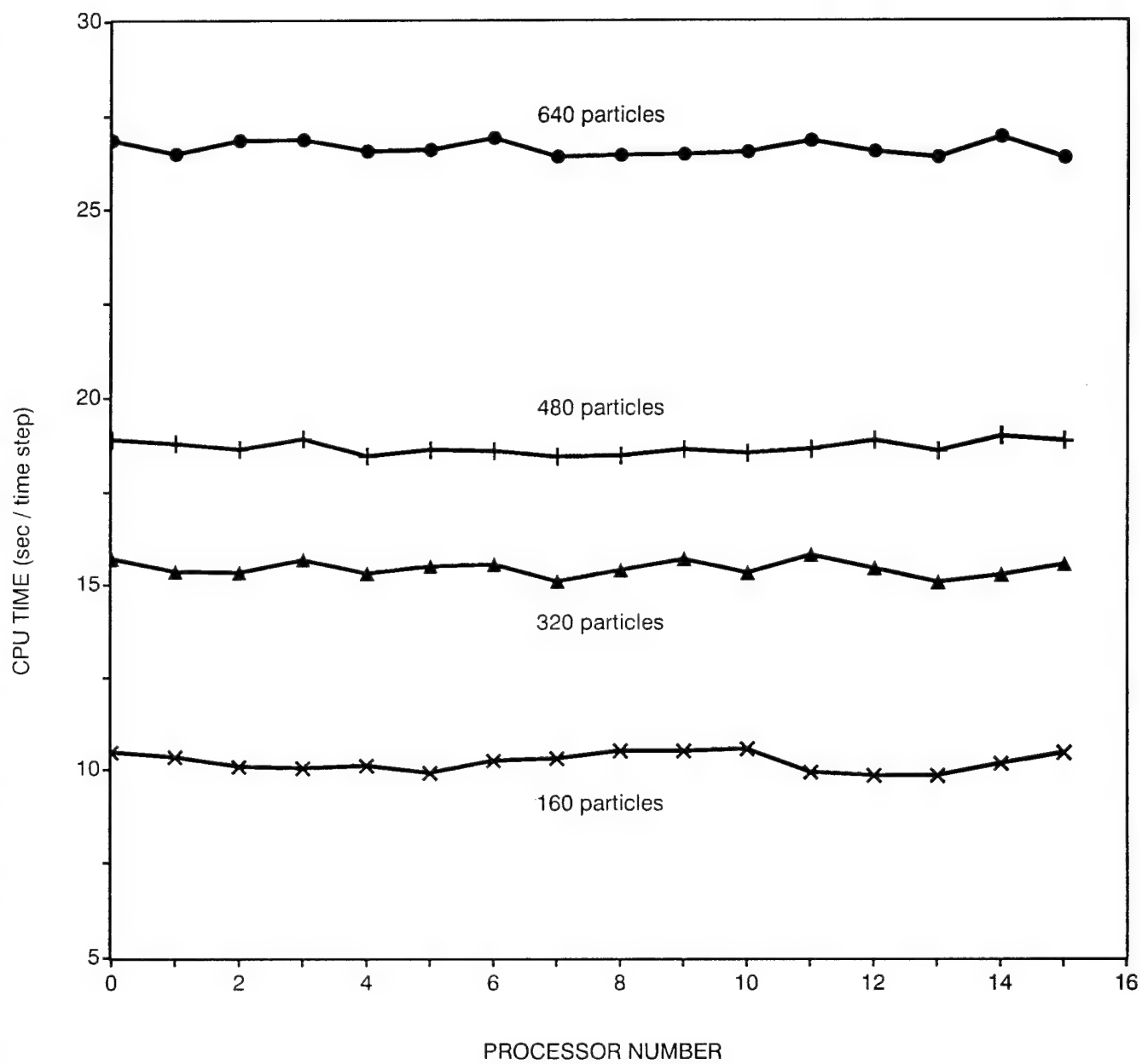Figure 11. Number of particles assigned to each processor under dynamic allocation scheme.

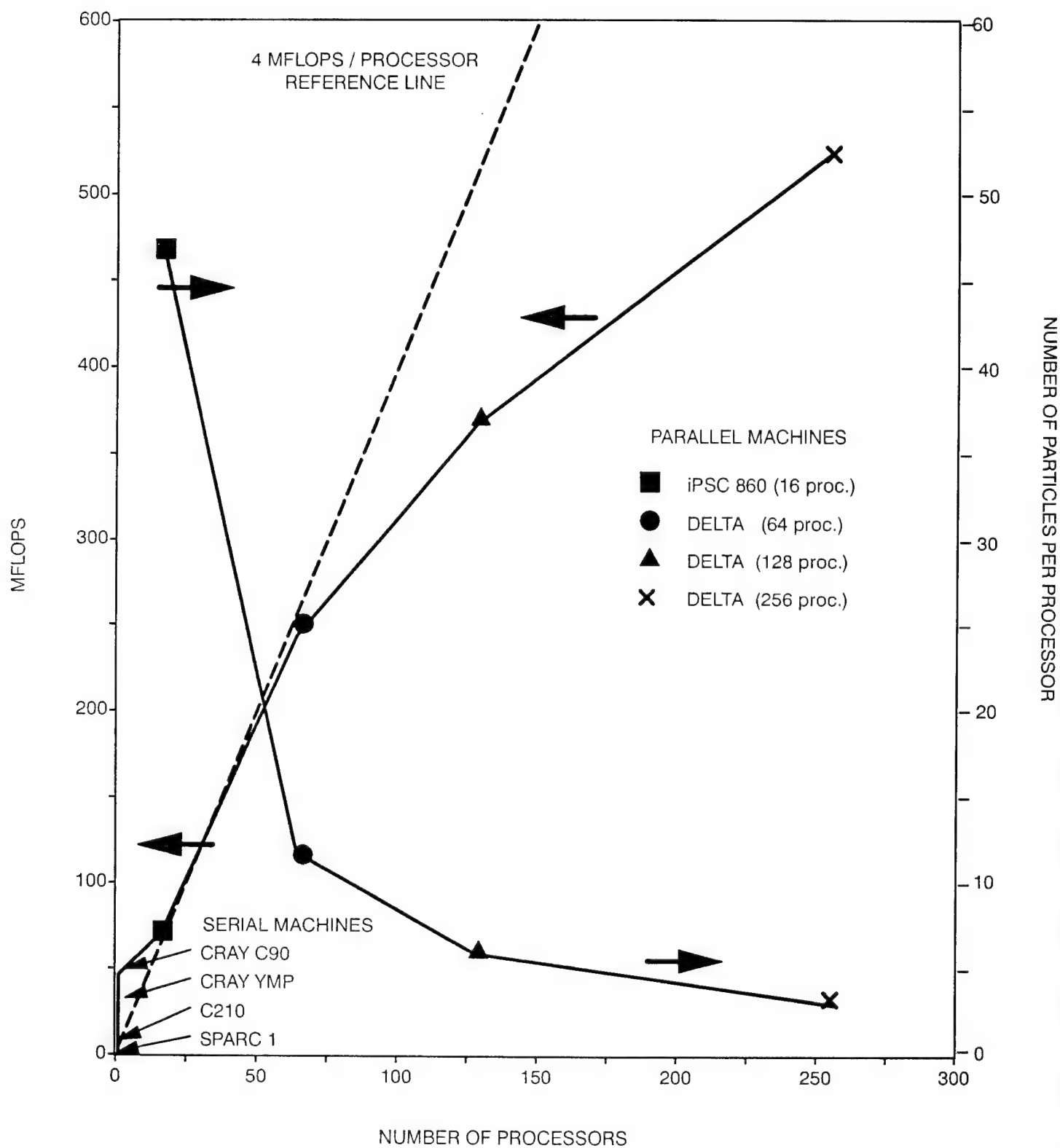Figure 12. Load balance resulting from dynamic allocation per Fig. 11.

Figure 13. Performance of PaSR algorithm on serial and parallel computers for CO/H_2 fuel, 1 atm, 1000K inlet, 762 particles.

Table II. "Full" Kinetic Scheme used for Lean Methane Combustion in PaSR Model.

(Forward rate constant $k_f = A \, T^b \, e^{-E/RT}$, moles$-cm-s-$K; E units: cal/mole)

No.	Reaction	A	b	E
1.	CH4(+M)=CH3+H(+M)	6.30E+14	0.0	104000.0
	Low pressure limit:	6.30E−03	0.0	18000.0
2.	CH4+O2=CH3+HO2	7.90E+13	0.0	56000.0
3.	CH4+H=CH3+H2	2.20E+04	3.0	8750.0
4.	CH4+O=CH3+OH	1.60E+06	2.4	7400.0
5.	CH4+OH=CH3+H2O	1.60E+06	2.1	2460.0
6.	CH2O+OH=HCO+H2O	7.53E+12	0.0	167.0
7.	CH2O+H=HCO+H2	3.31E+14	0.0	10500.0
8.	CH2O+M=HCO+H+M	3.31E+16	0.0	81000.0
9.	CH2O+O=HCO+OH	1.81E+13	0.0	3082.0
10.	HCO+OH=CO+H2O	5.00E+12	0.0	0.0
11.	HCO+M=H+CO+M	1.60E+14	0.0	14700.0
12.	HCO+H=CO+H2	4.00E+13	0.0	0.0
13.	HCO+O=OH+CO	1.00E+13	0.0	0.0
14.	HCO+O2=HO2+CO	3.00E+12	0.0	0.0
15.	CO+O+M=CO2+M	3.20E+13	0.0	−4200.0
16.	CO+OH=CO2+H	1.51E+07	1.3	−758.0
17.	CO+O2=CO2+O	1.60E+13	0.0	41000.0
18.	CH3+O2=CH3O+O	7.00E+12	0.0	25652.0
19.	CH3O+M=CH2O+H+M	2.40E+13	0.0	28812.0
20.	CH3O+H=CH2O+H2	2.00E+13	0.0	0.0
21.	CH3O+OH=CH2O+H2O	1.00E+13	0.0	0.0
22.	CH3O+O=CH2O+OH	1.00E+13	0.0	0.0
23.	CH3O+O2=CH2O+HO2	6.30E+10	0.0	2600.0
24.	CH3+O2=CH2O+OH	5.20E+13	0.0	34574.0
25.	CH3+O=CH2O+H	6.80E+13	0.0	0.0
26.	CH3+OH=CH2O+H2	7.50E+12	0.0	0.0
27.	CH2+H=CH+H2	4.00E+13	0.0	0.0
28.	CH2+O=CO+H+H	5.00E+13	0.0	0.0
29.	CH2+O2=CO2+H+H	1.30E+13	0.0	1500.0
30.	CH+O=CO+H	4.00E+13	0.0	0.0
31.	CH+O2=CO+OH	2.00E+13	0.0	0.0

32.	CH2CO+H=CH3+CO	7.00E+12	0.0	3000.0
33.	CH2CO+O=HCO+HCO	2.00E+13	0.0	2300.0
34.	CH2CO+OH=CH2O+HCO	1.00E+13	0.0	0.0
35.	CH2CO+M=CH2+CO+M	1.00E+16	0.0	59250.0
36.	HCCO+H=CH2+CO	3.00E+13	0.0	0.0
37.	HCCO+O=CO+CO+H	1.20E+12	0.0	0.0
38.	HO2+CO=CO2+OH	5.80E+13	0.0	22934.0
39.	H2+O2=2OH	1.70E+13	0.0	47780.0
40.	OH+H2=H2O+H	1.17E+09	1.3	3626.0
41.	H+O2=OH+O	2.00E+14	0.0	16800.0
42.	O+H2=OH+H	1.80E+10	1.0	8826.0
43.	H+O2+M=HO2+M	2.10E+18	−1.0	0.0

H2O Enhanced by 2.1, CO2 Enhanced by 5.0, H2 Enhanced by 3.3,

CO Enhanced by 2.0, O2 Enhanced by 0.0, N2 Enhanced by 0.0

44.	H+O2+O2=HO2+O2	6.70E+19	−1.4	0.0
45.	H+O2+N2=HO2+N2	6.70E+19	−1.4	0.0
46.	OH+HO2=H2O+O2	5.00E+13	0.0	1000.0
47.	H+HO2=2OH	2.50E+14	0.0	1900.0
48.	O+HO2=O2+OH	4.80E+13	0.0	1000.0
49.	2OH=O+H2O	6.00E+08	1.3	0.0
50.	H2+M=H+H+M	2.23E+12	0.5	92600.0

H2O Enhanced by 6.0, H Enhanced by 2.0, H2 Enhanced by 3.0

51.	O2+M=O+O+M	1.85E+11	0.5	95560.0
52.	H+OH+M=H2O+M	7.50E+23	−2.6	0.0

H2O Enhanced by 2.0

53.	H+HO2=H2+O2	2.50E+13	0.0	700.0
54.	HO2+HO2=H2O2+O2	2.00E+12	0.0	0.0
55.	H2O2+M=OH+OH+M	1.30E+17	0.0	45500.0
56.	H2O2+H=HO2+H2	1.60E+12	0.0	3800.0
57.	H2O2+OH=H2O+HO2	1.00E+13	0.0	1800.0
58.	N+O2=NO+O	6.40E+09	1.0	6280.0
59.	N+OH=NO+H	3.80E+13	0.0	0.0
60.	N+NO=N2+O	3.30E+12	0.3	0.0
61.	N+CO2=NO+CO	1.90E+11	0.0	3400.0
62.	NO+HO2=NO2+OH	2.10E+12	0.0	−480.0
63.	NO2+M=NO+O+M	1.10E+16	0.0	66000.0
64.	NO2+H=NO+OH	3.50E+14	0.0	1500.0
65.	NO2+O=NO+O2	1.00E+13	0.0	600.0

66.	HNO+M=H+NO+M	1.50E+16	0.0	48680.0
	H2O Enhanced by 6.0, H2 Enhanced by 2.0, O2 Enhanced by 2.0,			
	N2 Enhanced by 2.0			
67.	HNO+H=H2+NO	5.00E+12	0.0	0.0
68.	HNO+OH=NO+H2O	3.60E+13	0.0	0.0
69.	N2O=N2+O	2.82E+16	−1.6	62130.0
70.	N2O+H=N2+OH	7.60E+13	0.0	15200.0
71.	N2O+O=NO+NO	1.00E+14	0.0	28200.0
72.	N2O+O=N2+O2	1.00E+14	0.0	28200.0
73.	NCO+M=N+CO+M	3.10E+16	−0.5	48000.0
74.	NCO+O=NO+CO	5.60E+13	0.0	0.0
75.	NCO+OH=NO+CO+H	1.00E+13	0.0	0.0
76.	NCO+N=N2+CO	2.00E+13	0.0	0.0
77.	NCO+NO=N2O+CO	1.00E+13	0.0	−390.0
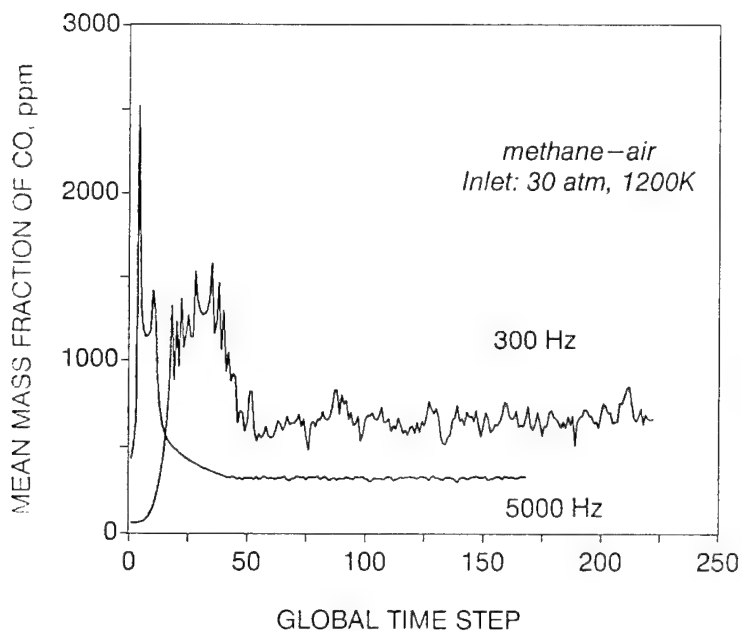
(a) Convergence of PaSR to stochastic steady state. Notice the greater level of turbulence in CO (and others) at the lower frequency (nearer blowout at these conditions).
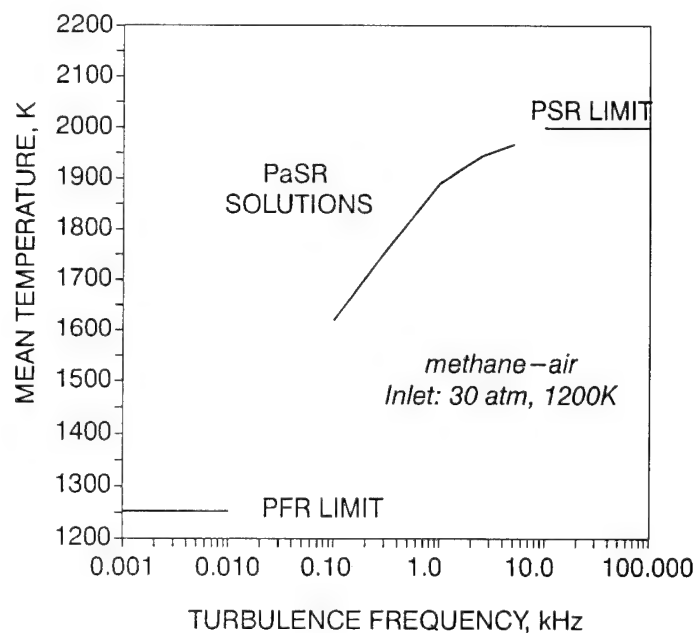
(b) Mean PaSR temperature and limit values. Gas–turbine combustors are being pushed towards the higher mixing rates, or else the blowout (extinction) threshold will be crossed.
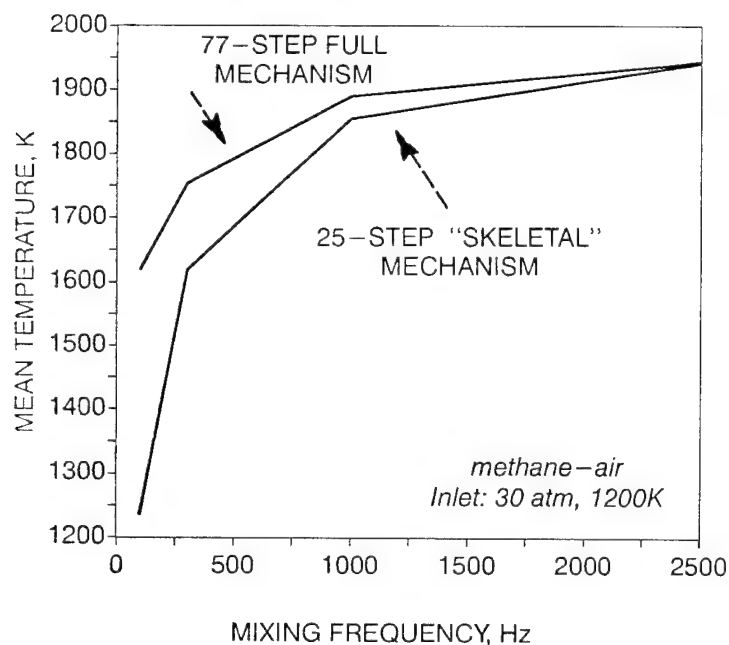
(c) Comparison of skeletal and full schemes. The 25–step skeletal scheme blows out prematurely. The derivative 4–step reduced scheme blew out at all frequencies.
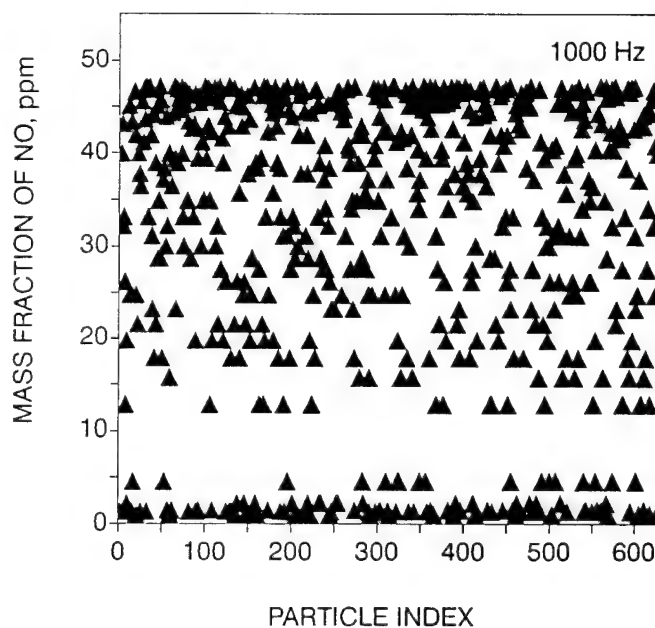
(d) Scatterplot of NO in the 1000 Hz ensemble after stochastic steady state is reached. Note wide distribution of NO. Corresponding scatterplots show wide variations in CO, CH_x and temperature.

Figure 14. Selected results from the "PaSR" model.

2.7 Assessment Of A 3-Variable Reduced Scheme For Complex Fuel

Most research in modeling is conducted with simple fuels, such as CO/H_2 mixtures or CH_4. However, jet engines burn higher hydrocarbons of typical composition C_nH_m with $n \simeq 10$ and $m \simeq 20$. The detailed kinetics of the oxidation mechanism are unknown. Even if they were known, computationally tractable kinetic schemes would be required for these fuels. Quasi-global schemes have been used in the past for engine applications [Edelman and Harsha (1978)], as well as for stirred reactors [Duterque (1981)] and laminar flames [Westbrook and Dryer(1981)]. Recent experimental data offer much detail on the intermediates formed in oxidation of kerosene in a jet-stirred reactor, thereby guiding the formulation of pyrolysis models [Gueret et al. (1990)].

The four- and five-variable schemes [e.g., Seshadri and Peters (1990)] are not worth the additional computational burden, given the empiricism in the global pyrolysis rate for complex fuels as well as the shortcomings of the four-step scheme demonstrated above in the PaSR. Hence, here we will develop a three-variable scheme that explicitly permits and retains a global pyrolysis rate.

To realistically assess a reduced kinetic scheme, the testbed must reproduce the microscale turbulent environment of the burner, or at least that of the CFD methodolgy in which the reduced scheme will be employed. To this end, the Partially Stirred Reactor ("PaSR") model is used, taking advantage of characteristics such as (i) its behavior is bounded by the perfectly stirred reactor (PSR) and the plug flow reactor (PFR), providing a set of checks on the model; (ii) at the high-frequency end, it provides a turbulence environment typical of highly turbulent combustors [Correa (1989)] namely, those in the *distributed reaction zone regime* rather than in the weaker *laminar flamelet regime,* and (iii) the joint velocity-scalar(s) pdf transport equation for multi-dimensional Monte Carlo CFD degenerates to the PaSR within each computational cell.

Following assessment in the PaSR over the entire range of mixing frequencies possible, a reduced scheme can be implemented in the multi-dimensional pdf/CFD model, and those predictions can be compared with data (from "real-world" inhomogeneous flow). This approach will provide the combustor designer with a predictive methodology that has been validated, to the maximum extent, at each step.

Since detailed kinetic schemes for complex fuels are unavailable, as discussed above, the baseline or "starting" kinetic scheme is initiated by an irreversible global pyrolysis reaction [Correa (1994 b)]

$$C_nH_m + (n/2) O_2 \rightarrow n\ CO + (m/2)\ H_2 \tag{4}$$

whose rate can be a function of the equivalence ratio; chain-branching (or "shuffle") reactions such as

$$CO + OH \leftrightarrows CO_2 + H \tag{5}$$

$$H_2 + O \leftrightarrows OH + H \tag{6}$$

$$H + O_2 \leftrightarrows OH + O \tag{7}$$

$$OH + OH \leftrightarrows H_2O + O \tag{8}$$
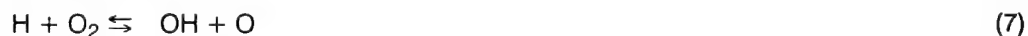
and recombination reactions such as

$$H_2 + M \rightarrow H + H + M \tag{9}$$

$$O_2 + M \rightarrow O + O + M \tag{10}$$

$$H + OH + M \rightarrow H_2O + M \tag{11}$$
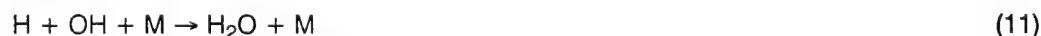
Standard rates are used for the elementary reactions (5)-(11).

29

Multi—step schemes contain too many variables (species plus enthalpy) to be tractable in CFD. Hence the number of variables must be reduced. Since the multi—step pyrolysis of lower hydrocarbons has, of necessity, already been replaced by the assumed single—step pyrolysis of the complex fuel, a good start has been made toward a reduced mechanism. Here partial equilibrium in the radical pool is used to further eliminate (chain—branching) steps.

For purposes of this development, we assume that "air" consists of 21% O_2 and 79% N_2, by volume, and that the initial reactants are exclusively the fuel (C_nH_m) and air. Furthermore, the only species in the system are C_nH_m, O_2, N_2, CO, H_2, CO_2, H_2O, O, OH, and H. Define $W_f \equiv (nW_C + mW_H)$ and $W_a \equiv (W_{O2} + 3.76W_{N2})$, where W_i is the molecular weight of species "i" (except that W_a is not the mean molecular weight of air). This system is described in terms of three variables: the mixture fraction ξ, the fuel mass fraction Y_f, and a composite radical pool variable Y^*. The ranges of the three variables ξ, Y_f and Y^* follow and will show that all possible thermochemical states fall within a tetrahedron in this three—dimensional $(\xi - Y_f - Y^*)$ space.

The first variable is a conserved scalar called the mixture fraction ξ, which is derived by normalizing the elemental mass fractions, Z_i, by the values in the fuel and air streams.

$$\xi = \frac{Z_i - Z_i^a}{Z_i^f - Z_i^a} \tag{12}$$

Superscripts a and f refer to the air and fuel streams, respectively. ξ is conserved because elements are unchanged by chemical reaction; likewise, the total (chemical plus sensible) enthalpy is conserved under reaction and can be mapped into ξ:

$$\xi = \frac{h - h^a}{h^f - h^a} \tag{13}$$

By construction, therefore, $0 \le \xi \le 1$.

The second variable is the fuel mass fraction Y_f, $Y_f^{min}(\xi) \le Y_f \le Y_f^{max}(\xi)$. The upper bound is set by having all the elements present in the initial reactants, i.e., $Y_f^{max}(\xi) = \xi$. The lower bound $Y_f^{min}(\xi)$ is set by the availability of O_2 to convert the maximum possible amount of C to CO and H_2 (not to CO_2 and H_2O).

The third variable is a composite Y^*, defined such that $\sigma^* \equiv \sigma_{H2} + \sigma_{CO}$, where $\sigma_j \equiv Y_j / W_j$ is the mole number of species "j." The bounds on Y^* follow from the bounds on CO and H_2 [Correa (1993 c)].

By considering the bounds on these three variables, the allowable $\xi - Y_f - Y^*$ space within which the reduced chemistry scheme must lie is obtained as a tetrahedron (Fig. 15).

Post—steady—state ensemble—mean quantities obtained from the PaSR model, using the starting and the reduced schemes, are shown in Figure 16. In each case, the independently computed high—frequency limit (PSR) and low—frequency limit (PFR convoluted with the theoretical age distribution) are also shown. All PaSR predictions lie smoothly between these limits, providing a set of checks on the model. Several points can be made:

(1) The global pyrolysis rate in the starting scheme does not yield complete combustion, appropriate for a heavy hydrocarbon under present circumstances. The low—frequency limit has only a 360K temperature rise; mixing is required to accelerate ignition of the incoming reactants, but even in the high—frequency mixing limit, the PSR temperature rise is only 860K and not the 1500K equilibrium rise. The assumed rate

30

can be altered to produce other results, if desired.

(2) The agreement between the starting scheme and the reduced scheme is excellent on the mean temperature (Fig. 16a) and on the mean fuel mass fraction (Fig. 16b), at all frequencies from 10 to 1000 Hz. The agreement on fuel mass fraction is not surprising since fuel pyrolysis is explicitly recognized as a degree—of—freedom in the reduced scheme. The latter is a desirable feature.

(3) The agreement on mean Y^*, which is the combined variable based on the CO and H_2 mole numbers, is not as good (Fig. 16c). Potential contributors to this discrepancy are the integration error, the coarseness in the look—up table, and the assumption of partial equilibrium. These factors can be examined in turn. First, the integration time step δt is small enough ($\delta t = 0.2\,\mu s \ll 1 / w^{max}$) to resolve the fastest rates in the system; in fact, simulations with smaller time steps gave the same results to several significant figures. Second, examination of the 1000 Hz ensemble shows that most of the particles are adjacent to the minimum Y^* boundary; hence, the coarseness of the grid in the Y^* direction (21 uniformly spaced points between $Y^{*,min}$ and $Y^{*,max}$) contributes to the discrepancy. This error can be reduced at the straightforward expense of adding points to the table in the Y^* direction. Third, the assumption of partial equilibrium in reactions 5—8 is not strictly correct under conditions where significant amounts of fuel are present; hence, it is responsible in part for the discrepancies between the starting and reduced schemes.

On balance, the reduced scheme exhibits encouraging performance. Recent data on the intermediates formed in the oxidation of kerosene in a jet—stirred reactor [Gueret et al. (1990)] will guide further development.
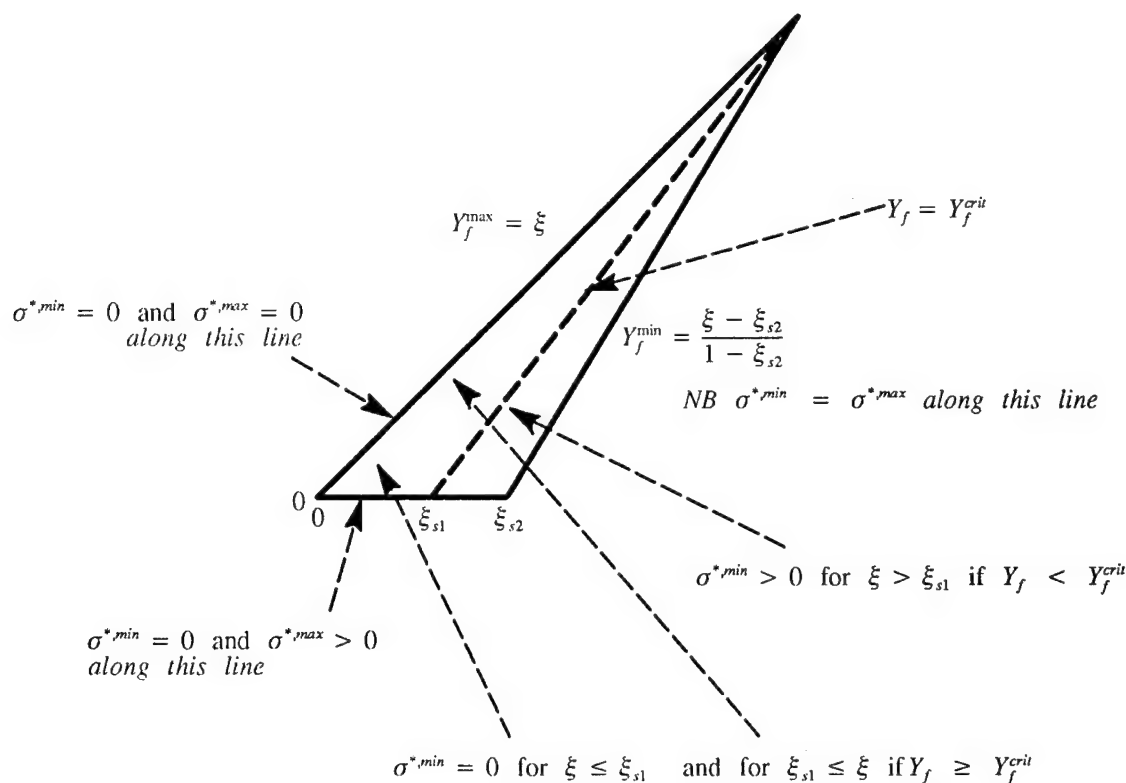
Figure 15. Depiction of allowable $\xi - Y_f - \sigma^*$ space in $\xi - Y_f$ plane.
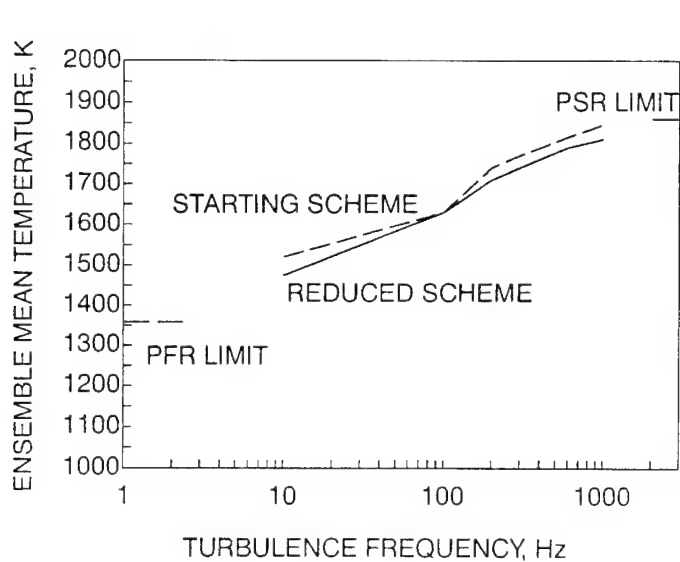
(a) Mean temperature.
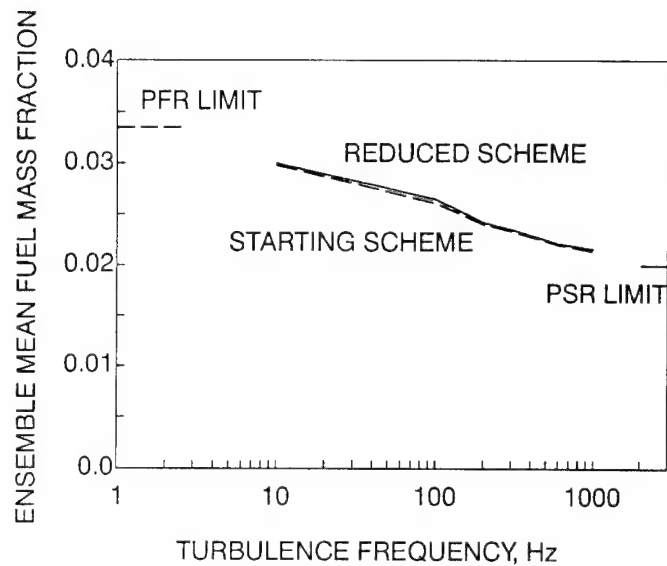
(b) Mean fuel mass fraction.
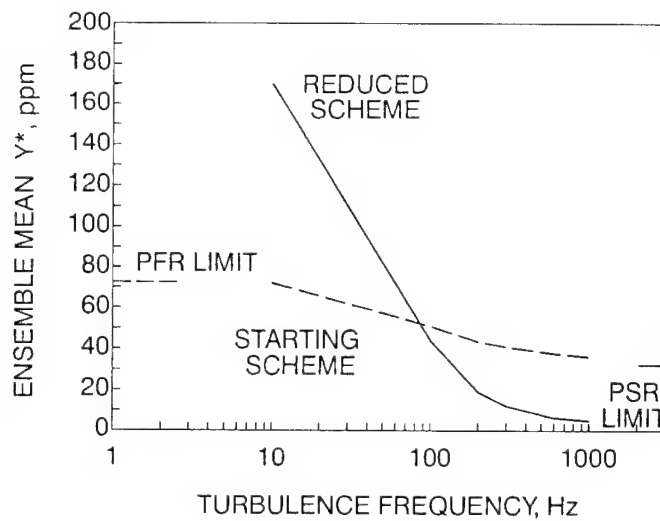
(c) Mean Y*, combined variable based on the CO and H_2 mole numbers.

Figure 16. Comparison of ensemble–mean quantities obtained from the PaSR model using the starting and the reduced schemes for a C_nH_m fuel. The PFR and PSR limits were obtained using the starting scheme and independent codes.

32

2.8 Direct Comparison of Mixing Models

Because reactions introduce at least one chemical time scale into the flow, the ratio of a characteristic mixing time to a characteristic chemical time (the Damkohler number, Da) becomes useful to classify the regime. If $Da \gg 1$ the system is in the flamelet regime where mixing models can be very inaccurate [Chen and Kollmann (1990)]. Concerns arise because pair—exchange models treat mixing and chemistry as sequential rather than simultaneous events, which can result in non—physical behavior. For example, consider two fluid particles which are outside the scalar(s)' range of chemical reactivity, both individually and in the mean. Some chemical reactions should occur in the process of mixing through the reactive regime; however, some models will return the non—reactive mean and hence mixing will take place without chemical reaction. If $Da \ll 1$ the system is in the "distributed combustion" regime, and reactions do not influence the turbulence to a significant extent. In reality, combustion proceeds through a multi—step reaction mechanism with a wide range of Damkohler numbers potentially spanning the gamut from distributed to flamelet behavior. Hence, little of useful generality can be said regarding scalars which react according to a realistic chemical kinetic scheme. Numerical experiments are needed to assess mixing models in this context.

The IEM model was advanced as being appropriate in Lagrangian calculations (such as particle tracking Monte Carlo calculations) of turbulent reacting flow [Meyers and O'Brien (1980)]. However, it has certain peculiarities such as the shape—preserving nature of the relaxation of the initial pdf of a conserved scalar undergoing mixing. Hence, it is of interest to compare it with other mixing models in the context of turbulent combustion. In particular, self—igniting combustion is a good test both for practical reasons — many important combustion systems such as those in gas—turbines are aerodynamically stabilized by intense mixing of products with reactants — as well as theoretical reasons, since a different set of time scales may be operative in the ignition phase.

The objective of this part of the study was to compare the Curl (1963) model, a modified Curl model developed by Dopazo (1979) and Janicka et al. (1979), and the "Interaction—by—Exchange—with—the—Mean" (IEM) mixing model [Borghi (1988)] which was introduced above.

(i) The Curl (1963) model randomly chooses N_{mix} pairs of particles, mixes them by averaging their scalar values, and finally returns them to the ensemble. The mean is unchanged, whereas the variance decreases, in the inert case. Illustrating the case for a conserved scalar ξ, consider the mixing of one pair (out of N_{mix} pairs of particles which are mixed at each time step, where N_{mix} is given below). Let the two participating particles have the values ξ_1 and ξ_2 at the beginning of the time step. Then, according to the Curl model, the values at the end of the step (superscript "new") are

$$\xi_1^{new} = \xi_2^{new} = \frac{1}{2} (\xi_1 + \xi_2) \tag{14a}$$

To produce the correct decay rate for the variance of a conserved scalar,[7]

$$N_{mix} = 2 \ N_p \ \omega \ \Delta t \tag{14b}$$

Weaknesses of the Curl model have been described in detail, in the case of the evolution of the pdf of a conserved scalar [Pope (1982)]. In particular, the Curl model never yields a continuous distribution when starting with a pdf which is composed of delta functions; hence, the higher moments of the pdf are never correct.

33

Following mixing, the mass fractions and temperature of each particle in the ensemble are advanced in time by integration of the chemical kinetics equations.

(ii) The Modified Curl model also randomly chooses pairs of particles, but mixes them by averaging their scalar values in a weighted manner [Dopazo (1979), Janicka et al. (1979), Pope (1982)]. The two participating particles in the above example will have the new values

$$\xi_1^{new} = (1 - \alpha)\xi_1 + \frac{1}{2}\alpha(\xi_1 + \xi_2) \tag{15a}$$

$$\xi_2^{new} = (1 - \alpha)\xi_2 + \frac{1}{2}\alpha(\xi_1 + \xi_2) \tag{15b}$$

where the weight α is varied randomly between zero and one according to the flat pdf $P(\alpha)=1$; note that other choices for $P(\alpha)$ could have been made. With $\alpha = 0$ the particles do not mix, and with $\alpha=1$ the Curl model is reproduced. To produce the correct decay rate, N_{mix} must be

$$N_{mix} = 3 \ N_p \ \omega \ \Delta t \tag{15c}$$

Once again, the post−mixing mass fractions and temperature of each particle in the ensemble are advanced in time by integration of the chemical kinetics equations.

The modified Curl model addresses some of the weaknesses of the original Curl model; however, Pope (1982) demonstrated that although it does indeed yield a continuous pdf when starting with a distribution which is composed of delta functions (provided that $P(\alpha)$ is continuous), that pdf is not the expected Gaussian. The peak and the tails of the pdf exceed those of the Gaussian.

(iii) The IEM model relates each particle to the ensemble, rather than to a partner. The equations were given above and will not be repeated here. The IEM model has a characteristic which is evident from its parent pdf evolution equation. For a conserved scalar in a homogeneous system without inflow or outflow, the pdf $P(\xi,t)$ evolves according to

$$\frac{\partial P}{\partial t} - \frac{\partial}{\partial \xi}[(\xi - \bar{\xi})P] = 0 \tag{16a}$$

where $\bar{\xi}$ is the mean; the mean does not change in this situation. The general solution is

$$P(\xi, t) = \frac{fn[t + \ln(\xi - \bar{\xi})]}{\xi - \bar{\xi}} \tag{16b}$$

where fn is a function defined by the initial condition $P(\xi,0)$. It is clear from Eq. 16 (b) that the IEM model relaxes the pdf (of a conserved scalar) in a shape−preserving manner and does not approach the expected Gaussian in the general case.

All three mixing models fail to yield the Gaussian expected of a conserved scalar pdf in the limit of large time; however, as mentioned above, the significance of this failure is not obvious in the reacting case and motivates the present work.

First we confirm that the mixing models agree identically on the decay of the variance of a conserved scalar, in a system without inflow or outflow. Consider the evolution of the pdf of a conserved scalar, $P(\xi,t)$. Let the mixing occur at a rate such that the variance σ^2 decays per $d\sigma^2/dt=-2\omega\sigma^2$ (i.e., the standard deviation σ decays according to $d\sigma/dt=-\omega\sigma$). Each of the three ensembles is marched forward in time, without chemical reactions.

Initially symmetric and asymmetric pdf's were examined. Figure 17 shows typical results for the pre-scribed decay rate ω=1000 s^{-1}. There are no discernible differences between the models, all of which re-produce the 1000 s^{-1} decay rate. We conclude that the three mixing models are equivalent (up to the vari-ance) for the case of a conserved scalar. This calculation is merely a test of the present implementation; the results of Fig. 17 are expected [Pope (1982)].

Next, inflow, outflow and chemical reactions are reactivated in the PaSR.

The fuel is taken to be a mixture of 50%CO/50%H$_2$ (by vol.). The kinetic scheme consists of 11 species and 23 reactions (Table III). The inlet conditions are 1 atm and 900K. The stoichiometry of the premixed inflow leads to a PSR temperature of 1740K at a residence time of 5 ms (1800K in equilibrium), but to blowout in a PFR. The PaSR mixing frequency was varied in the range $10 - 10^4$ Hz, by factors of $\sqrt{10}$; it has been shown that this range more than covers the mixing frequencies encountered in a practical combustor [Cor-rea and Braaten (1993)]. The computations are run keeping the PaSR volume and the mass flow rate fixed, so the residence time τ varies with the mean density according to $\tau \equiv \overline{\varrho}V/m$, where $\overline{\varrho}$ is the mean density, V is the reactor volume and m is the mass flow rate.

In the interest of brevity, only the temperature will be discussed here. Figure 18 shows the evolution of the mean temperature. Results are shown for two mixing frequencies, which were chosen to differentiate between the behavior of the models as blowout is approached. The mean temperature attains a stochasti-cally steady state. It is clear that the IEM model sustains combustion at both the chosen frequencies, where-as the Curl and modified Curl models approach blowout at the lower frequency. The initial evolution is very similar for all three models: the PaSR, which was initialized with particles whose composition and tempera-ture were set to the PSR results, tends to cool down as the initial particles are replaced by incoming par-ticles. The Curl and modified Curl models exhibit a greater degree of fluctuations, which is not surprising as blowout is approached.

It should be noted that we present all frequencies including those which are lower than the ≥ 500 Hz expected of practical turbulent combustion. The models become increasingly similar in their conver-gence paths at higher frequencies, although the Curl and modified Curl models continue to exhibit a greater degree of fluctuations in the mean.

The pdf's of particle age, computed from the steady−state ensembles that were obtained using each of the three models at the two different frequencies which will be examined in detail below, are shown in the form of histograms in Fig. 19. Also shown is the theoretical pdf,

$$P(\psi) = \frac{1}{\tau} \exp(- \psi/\tau) \tag{17}$$

where the variable ψ is the age. All three models reproduce the theoretical pdf fairly well; the deviations are caused by the finite number of particles in the ensemble ($\approx$500).

Table III. Kinetic Mechanism Used for CO/H_2–Air Combustion.

(Forward rate constant $k_f = A\ T^b\ e^{-E/RT}$, moles–cm–s–K; E units: cal/mole)

No.	Reaction	A	b	E
1.	CO+O+M=CO2+M	3.20E+13	0.0	−4200.0
2.	CO+OH=CO2+H	1.51E+07	1.3	−758.0
3.	CO+O2=CO2+O	1.60E+13	0.0	41000.0
4.	HO2+CO=CO2+OH	5.80E+13	0.0	22934.0
5.	H2+O2=2OH	1.70E+13	0.0	47780.0
6.	OH+H2=H2O+H	1.17E+09	1.3	3626.0
7.	H+O2=OH+O	2.00E+14	0.0	16800.0
8.	O+H2=OH+H	1.80E+10	1.0	8826.0
9.	H+O2+M=HO2+M	2.10E+18	−1.0	0.0

H2O enhanced by 21.0, CO2 enhanced by 5.0, H2 enhanced by 3.3,

CO enhanced by 2.0, O2 enhanced by 0.0, N2 enhanced by 0.0

No.	Reaction	A	b	E
10.	H+O2+O2=HO2+O2	6.70E+19	−1.4	0.0
11.	H+O2+N2=HO2+N2	6.70E+19	−1.4	0.0
12.	OH+HO2=H2O+O2	5.00E+13	0.0	1000.0
13.	H+HO2=2OH	2.50E+14	0.0	1900.0
14.	O+HO2=O2+OH	4.80E+13	0.0	1000.0
15.	2OH=O+H2O	6.00E+08	1.3	0.0
16.	H2+M=H+H+M	2.23E+12	0.5	92600.0

H2O Enhanced by 6.0, H enhanced by 2.0, H2 enhanced by 3.0

No.	Reaction	A	b	E
17.	O2+M=O+O+M	1.85E+11	0.5	95560.0
18.	H+OH+M=H2O+M	7.50E+23	−2.6	0.0

H2O enhanced by 21.0

No.	Reaction	A	b	E
19.	H+HO2=H2+O2	2.50E+13	0.0	700.0
20.	HO2+HO2=H2O2+O2	2.00E+12	0.0	0.0
21.	H2O2+M=OH+OH+M	1.30E+17	0.0	45500.0
22.	H2O2+H=HO2+H2	1.60E+12	0.0	3800.0
23.	H2O2+OH=H2O+HO2	1.00E+13	0.0	1800.0

The mean temperature is displayed against the mixing frequency in Fig. 20. At high enough frequencies (>1000 Hz), all three models approach the PSR values. At lower frequencies, however, the pair−exchange models tend to blow out while the IEM model sustains combustion. On the basis of the results for the means, it may be provisionally concluded that the models are essentially similar at the high mixing frequencies of practical interest. This conclusion were tested in greater detail by examining pdf's and scatterplots.

The temperature pdf, obtained from the steady−state ensembles, shows a greater degree of bimodality between the inlet and near−PSR temperatures with the pair−exchange models than with the IEM model (Fig. 21) . These differences increase as the frequency drops below 100 Hz. New particles are clearly more quenched by the former models' sequential treatment of mixing and reaction than by the simultaneous treatment in the IEM model, accounting for the lower mean temperatures encountered above. We also note that the equations for the IEM model resemble those of the stirred reactor, which admits abrupt transitions (bifurcations) between lit and unlit states in high activation−energy systems. Hence it is not surprising that the IEM model approaches blowout in a more abrupt manner than the pair−exchange models. The three mixing models yield similar pdf's at the high temperature end.

These results indicate that the choice of mixing model is not critical in the distributed reaction regime of lean premixed combustion, as long as the turbulent mixing frequencies are above about 1000 Hz. Three−dimensional CFD calculations of practical high−intensity combustors indicate in−flame mixing frequencies of 1000 Hz and above. Hence, in such combustors, the differences between models are overwhelmed and blurred by the finite rates of the chemical reactions. The computational advantages of the IEM model, which is well suited to parallel computer architectures whether in the form of standalone machines or a networked cluster of workstations operating as a "virtual" parallel machine, make it the model of choice.

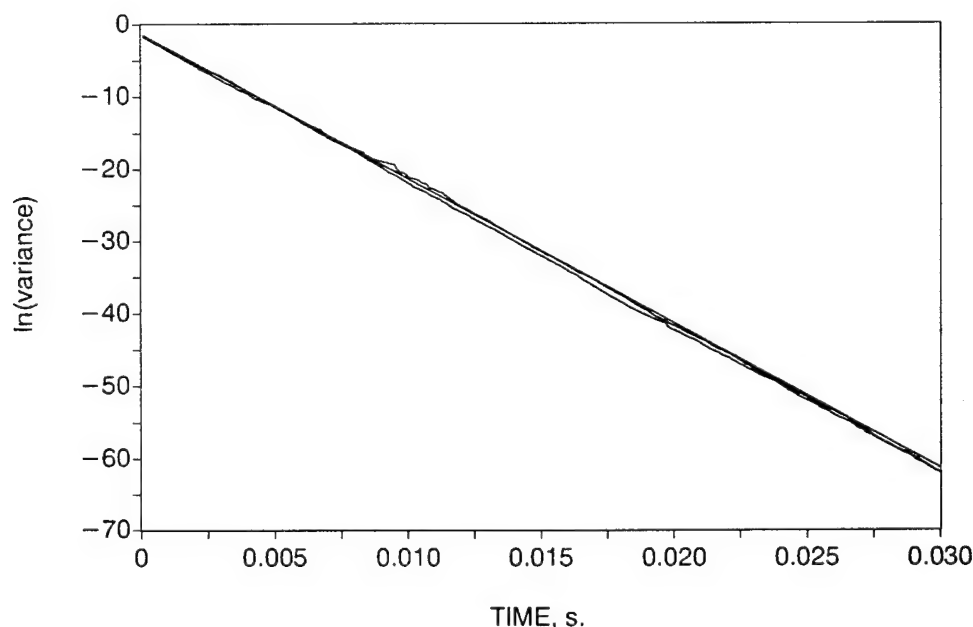Figure 17. The decay of the variance of a conserved scalar, computed using the three mixing models. 500 particles, ω=1000 Hz, Δt=0.1/ω.
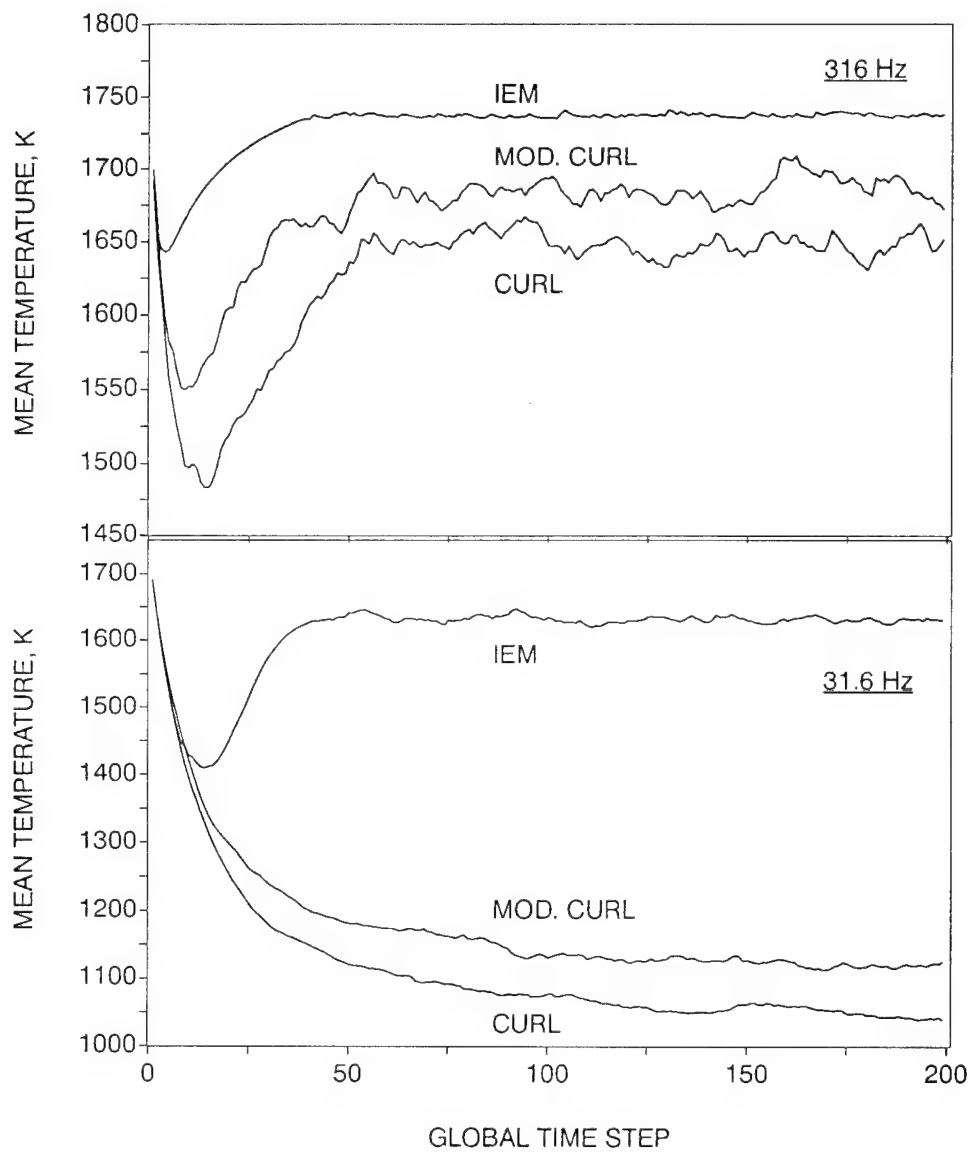
Figure 18. Evolution of mean temperature with the three mixing models, at two mixing frequencies.
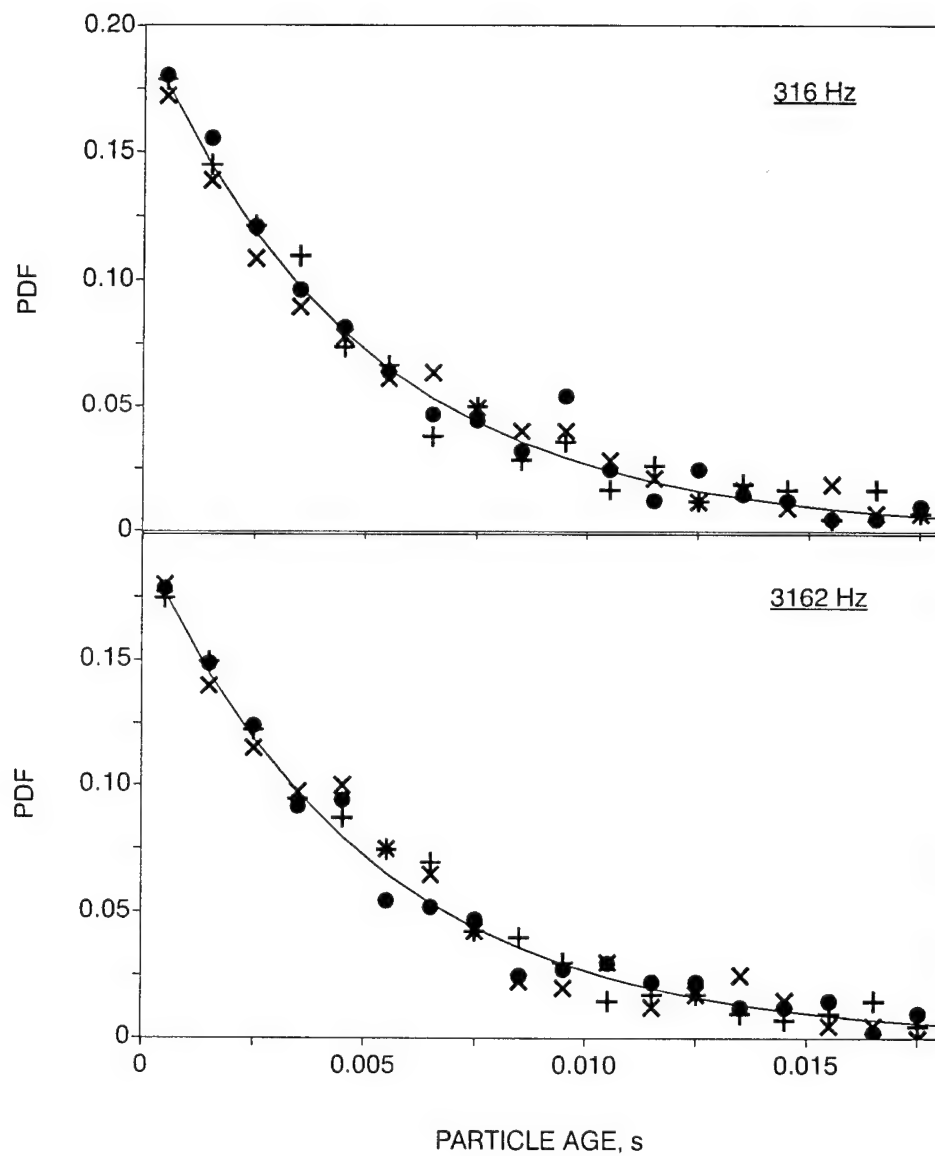
Figure 19. Pdf's of particle age. x Curl model; + Modified Curl model; ● IEM model. The solid line is the theoretical pdf for a 5 ms residence time.
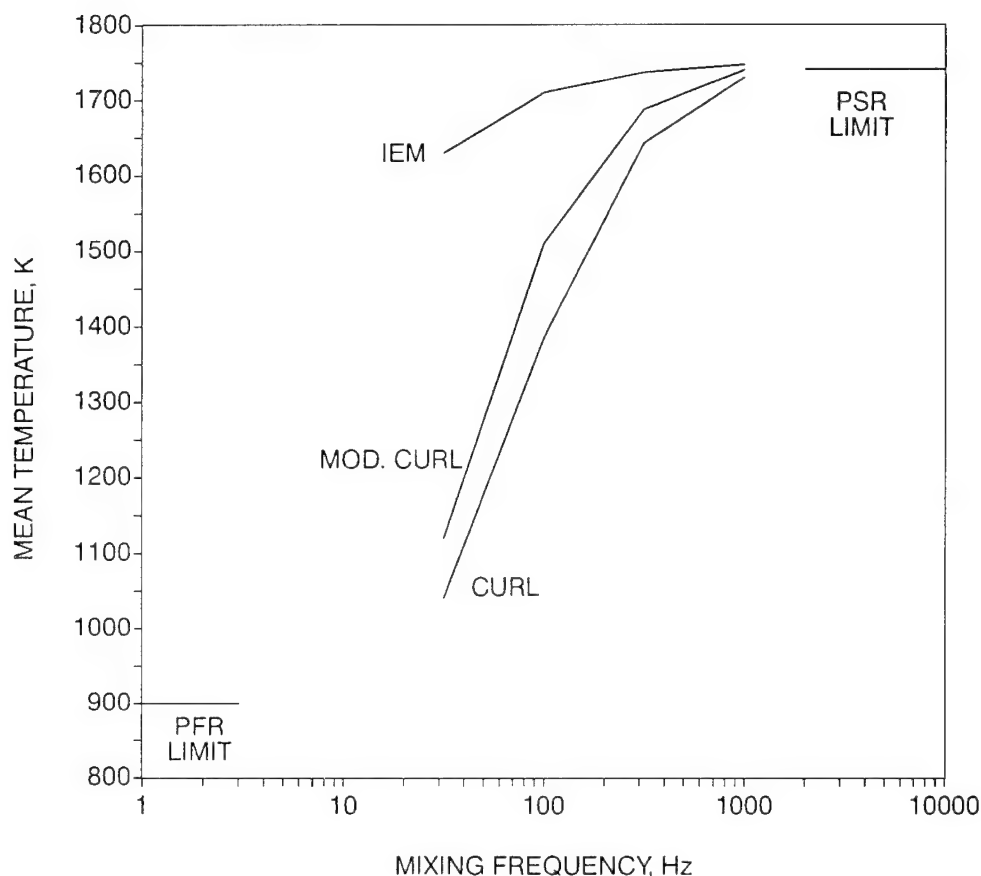
39

Figure 20. Variation of mean temperature with mixing frequency.

The PaSR has shown that as blowout is approached, differences arise between the above mixing models which are commonly used in CFD. Which is "right"? First, are PaSR results even of any general significance?

To put the PaSR in context, it is worthwhile to repeat one possible vision of a future combustion model. This future model will employ the Monte Carlo particle tracking/pdf transport approach to turbulence−chemistry interactions and be dynamically iterated with a complex−geometry mean flow/two−equation turbulence CFD model, as in Section 2.1. However, it will not use reduced chemistry but instead a full scheme with a large number of species (eventually, as many as 50). This degree of precision in the chemistry is required to address the issues of the day (NO_x down to the level of 5 ppm, CO, unburned hydrocarbons, flame stability under extreme conditions, and so on). Within each computational cell the system is spatially homogeneous but unmixed, as in the present PaSR. Since full chemistry is too expensive to use in calculations of general inhomogeneous flows at present, here we have in effect concentrated on turbulence−chemistry interactions in the single cell (i.e., on a single PaSR). Hence, data from inhomogeneous systems are not directly usable. Experimental data on a PaSR are needed to decide which model is most "right" physically and to make further choices on mixing closure.

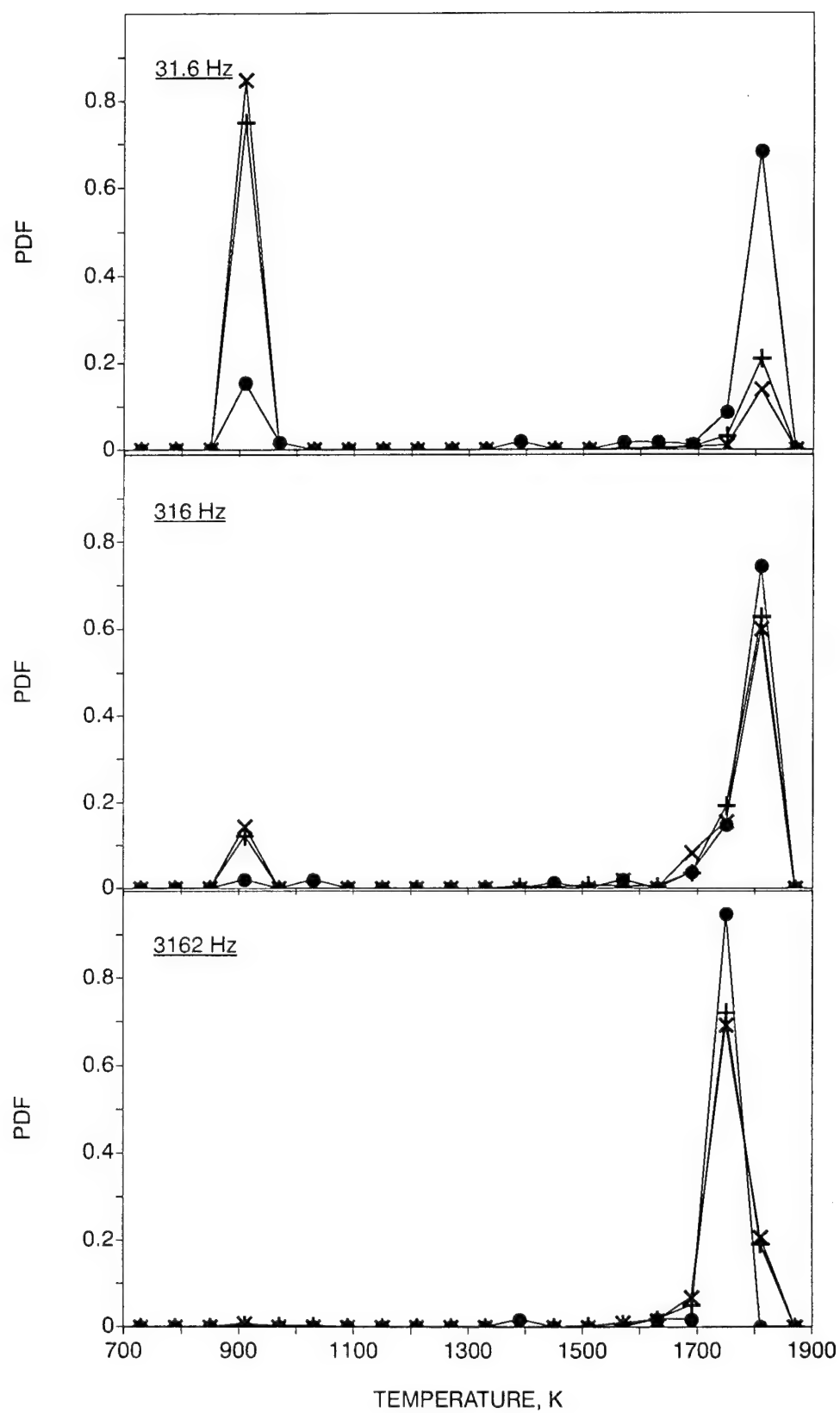Figure 21. Pdf of temperature at three selected mixing frequencies.

Section 3
CONCLUSIONS

We have conducted experiments on bluff–body stabilized flames of CO/H_2 and CH_4/air. By correcting for fluorescence, we have made Raman measurements in bluff–body CH_4–air flames; however, the errors in certain species (e.g., CO and CO_2) may be so large that models should not be changed on the basis of such data alone. This of course detracts severely from the utility of expensive laser–based measurement techniques. In refereed publications and in oral presentations, we have raised the consciousness of the university and industrial research community to this issue.

We have examined modeling approaches of varying complexity.
1. The assumed shape pdf model: it was dismissed because it is not extendable to multi–scalar chemistry.
2. The "conditional moment closure" model: it was dismissed because it is applicable only when the fluctuations about the conditional mean are small (i.e., as in low–intensity turbulent combustion).
3. The scalar pdf model, which does not treat the velocity part of the pdf. Instead this model uses standard turbulence modeling to supply the scalar (and momentum) fluxes. It is a reasonable engineering tool in 3D design, but it is not state–of–the–art in terms of research and hence cannot be used to develop advanced tools of the future.
4. The joint velocity–composition pdf transport model. During this contract period, we have extended joint pdf modeling from parabolic (jet) flames to elliptic (bluff–body recirculation–stabilized) flames as found in practical burners. The axisymmetric elliptic mean flow CFD model and the pdf model communicate with each other iteratively. The speedup achieved in parallelizing particle tracking pdf computations – accomplished in the present reporting period of this contract – shows that the pdf computations are tractable in practical design codes.

The Monte Carlo joint PDF/CFD model has been assessed by comparisons with Raman data on means and rms of mixture fraction, major species and temperature in non–premixed bluff–body stabilized CO/H_2 and CH_4 flames. For brevity and because most of the points were made in the subsequent CH_4 flame, the CO/H_2 flames were not discussed here. Details are available in Correa and Pope (1992). The CH_4 flame was discussed in detail, demonstrating several points:
1. The bluff body burner provides a strongly turbulent field leading to localized extinction, without the need for a pilot flame. Thus the two–stream nature of the problem is preserved, unlike many piloted jet flame studies where the composition or the excess enthalpy of the pilot flame can cause modeling difficulties. The present recirculation–stabilized flame is also much closer to practical burners.
2. Given the similarity in scatterplots, it is clear that the pointwise structure of the above bluff body flame and the piloted jet flame are quite similar. A greater degree of local extinction is measured here.
3. The limitations of pdf shape assumption, statistical independence of scalars, and gradient diffusion, are removed in this joint pdf model. The consequences can be seen in joint scatterplots and in convective fluxes.
4. The calculated CO scatterplots have maxima of 3% whereas the data peak at about 10%, well above the flamelet maxima. Similar 10% levels were measured another bluff body flame and in pilot–stabilized flames, and 2–3% peaks were predicted in the latter using the 4–step scheme. Hence this discrepancy on CO maxima has appeared in diverse circumstances (but always in combustion gases that are near local extinction). There are many potential contributors, including: (i) the assumption of a steady state for the radicals in the 4–step mechanism; (ii) the errors in Raman–based CO and CO_2 data; and (iii) neglect

of phenomena such as unsteady flamelets or micromixed gases (perfectly stirred reactors) which have been shown to lead to high CO. In intense turbulence, however, the microscale may be better simulated by spatially homogeneous systems.

It seems clear that CO is an important clue to the microstructure of highly turbulent combusting gases, and that accurate measurements will be critical.

The acquisition of Raman data and the 3−velocity/5−scalar joint pdf calculation in this bluff body methane flame took each "discipline" to the limits of the present state of the art. Any significant further progress is likely to require improvements in major species measurements, complementary velocity and minor species measurements, and parallel computers. Reduced chemistry schemes which relax steady−state assumptions (and are likely to require additional scalars) will have to be developed and assessed in simpler contexts.

We have shown that an intense combustion process should not be viewed as the motion of a high−speed flamefront; as the turbulence amplitude and frequency increase, the relevance of reaction−diffusion interfaces (flamefronts) decreases. Ultimately, the velocity field and the spatial structure become less important and a stirred reactor description would be more appropriate at the micro−scale level.

To the latter end, we developed the "PaSR" or partially stirred reactor model for spatially homogeneous (but not mixed) reacting flows. The PaSR offers an alternative to traditional evaluations in laminar flames, which are not relevant to turbulent combustion.

We have demonstrated that particle tracking pdf calculations are easily parallelized, whereas flow codes "prefer" vector computers. The parallel implementation was targeted at distributed memory MIMD (multiple instruction, multiple data set) computers such as the Intel iPSC/860 and Intel Delta. From the huge speed−up (factors of 100) in execution time, it is clear that such computations are indeed practical in the networked−workstation−intensive environment of the typical gas−turbine design community. It was also clear that distributed memory MIMD parallel architectures are well suited to the particle−tracking PaSR algorithm. This remains true so long as the turbulence model does not require continuous communication between "particles." Thus, the IEM model is preferable to pair−exchange models on parallel or networked computers.

We have used the PaSR model in first−ever studies of a full (27−species/77−reactions) methane oxidation scheme interacting with prescribed turbulence. The calculation involved 600 to 700 particles and therefore $\approx$ 20,000 o.d.e.'s. The PaSR smoothly merges into PSR and PFR limits as mixing frequency becomes large or small, respectively. The degree of turbulence in the time−histories of species is apparent, e.g., greatest for CO (among major species) as blowout is approached. The "skeletal" mechanism used as the basis for the 4−step reduced scheme in laminar flames cannot reproduce the full scheme's results at low frequency, where ignition chemistry becomes important.

We have also applied the PaSR to assess a 3−variable (in the non−premixed case) reduced chemistry scheme for a hypothetical heavy hydrocarbon. The agreement between the starting scheme and the reduced scheme was excellent on the mean temperature and on the mean fuel mass fraction. Fuel pyrolysis is explicitly recognized as a degree−of−freedom in the reduced scheme. The latter is a desirable feature. The agreement on mean Y^*, which is the combined variable based on the CO and H_2 mole numbers, was

43

not as good. Potential contributors to this discrepancy have been identified. On balance, the reduced scheme exhibits encouraging performance.

We have also used the PaSR to directly compare the IEM model, the Curl model, and the modified Curl model in the context of a full scheme in prescribed turbulence. The results indicate that the choice of mixing model is not critical in the distributed reaction regime of lean premixed combustion, so long as the turbulent mixing frequencies are above about 1000 Hz. Three–dimensional CFD calculations of practical gas–turbine combustors indicate in–flame mixing frequencies of 1000 Hz and above. Hence, in such combustors, the differences between mixing models are overwhelmed and blurred by the finite rates of the chemical reactions. The computational advantages of the IEM model, which is well suited to parallel computer architectures whether in the form of standalone machines or a networked cluster of workstations operating as a "virtual" parallel machine, make it the model of choice.

We have only briefly summarized the development and some key conclusions of the PaSR model. Many more results and sensitivity analyses are given in our refereed literature (Section 5). The PaSR model has also been adopted as an investigative tool by other researchers, e.g., at the University of Sydney and at UC–Berkeley.

Section 4
REFERENCES

Bilger, R.W., Twenty−Second International Symposium on Combustion, The Combustion Institute, Pittsburgh, PA, pp. 475−488, 1988.

Bowman, C.T., Twenty−Fourth Symposium (International) on Combustion, The Combustion Institute, Pittsburgh, PA, 1992, pp. 859−878.

Borghi, R., *Prog. Energy and Combust. Sci.,* 14, pp. 245−292, 1988.

Chen, J.−Y., Kollmann, W., and Dibble, R.W., *Combust. Sci. and Tech.,* 64, pp. 315−346, 1989.

Chen, J.−Y., and Kollmann, W., Twenty−Third Symposium (International) on Combustion, The Combustion Institute, Pittsburgh, PA, 1990, pp. 751−757.

Chen, J.−Y. and Dibble, R.W., *Combust. Sci. and Tech.,* 84, pp. 45−50, 1991.

Correa, S.M. and Shyy, W., *Prog. Energy and Combust. Sci.,* 13, pp. 249−292, 1987.

Correa, S.M., Gulati, A. and Pope, S.B., *Combust. Flame,* 72, pp. 159−173, 1988.

Correa, S.M. and Gulati, A.,"Local Extinction Mechanisms in Non−Premixed Turbulent Combustion," Final Report, AFOSR Contract F−49620−88−C−0066, August 1991.

Correa, S.M. and Pope, S.B., Twenty−Fourth Symposium (International) on Combustion, The Combustion Institute, Pittsburgh, PA, pp. 279−285, 1992.

Correa, S.M.,"Relevance of Non−premixed Laminar Flames to Turbulent Combustion," in *Major Research Topics in Combustion*, Hussaini, M.Y., Kumar, A., and Voight, R.G., Eds.,pp. 45−69, Springer−Verlag, 1992.

Correa, S.M. and Gulati, A., *Comb. and Flame,* 89, pp. 195−213, 1992.

Correa, S.M., *Combust. Sci. and Tech.,* 87, pp. 329−362, 1992.

Correa, S.M. and Pope, S.B., Twenty−Fourth Symposium (International) on Combustion, The Combustion Institute, Pittsburgh, PA, 1992, pp. 279−285.

Correa, S.M. and Braaten, M.E., *Combust. Flame,* 94, pp. 469−486, 1993.

Correa, S.M., *Combust. Flame,* 93, pp. 41−60, 1993.

Correa, S.M., "Models for High−Intensity Turbulent Combustion," *Comp. Sys. in Engg.,* Vol. 5, No. 2, pp. 135−145, 1994 a.

Correa, S.M., Gulati, A., and Pope, S.B.,"Raman Measurements and Joint PDF Modeling of a Non−Premixed Bluff Body−Stabilized Methane Flame," Twenty−Fifth Symposium (International) on Combustion, Irvine, CA, July 31 − August 5, 1994.

Correa, S.M.,"Assessment of a 3−Variable Reduced Kinetic Scheme in Prescribed Turbulence," in press *J. Prop. Power*, 1994 b.

Curl, R.L., *AlCh. E. J.,* 9, pp. 175−181, 1963.

Dibble, R.W., Starner, S.H., Masri, A.R., and Barlow, R.S., *App. Physics*, B51, pp. 1727−1731, 1990.

Dopazo, C., Phys. Fluids, 22:20−30, (1979).

Drake, M.C., Lapp, M. and Penney, C.M.,"Use of Raman Effect for Gas−Temperature Measurement," in *Temperature, Its Measurement in Science and Industry*, (J. F. Schooley, Ed.), 1982, Vol. 5, p. 631.

Duterque, J., Borghi, R., and Tichtinsky, H., *Comb. Sci. Tech., 26*, p. 1, 1981.Edelman, R.B. and Harsha, P.T., *Prog. Energy Comb. Sci., 4*, p. 1, 1978.

Gueret, C., Cathonnet, M., Boettner, J.−C., and Gaillard, F., Twenty−Third (International) Symposium on Combustion, The Combustion Institute, Pittsburgh, PA, pp. 211−216, 1990.

Janicka, J., Kolbe, W., and Kollmann, W., *J. Nonequil. Thermodyn.,* 4:47−56, (1979).

Kee, R.J., Rupley, F.M., and Miller, J.A., "Chemkin−II: A Fortran Chemical Kinetics Package for the Analysis of Gas−Phase Chemical Kinetics," SANDIA Report SAND89−8009, Sandia National Laboratories, Livermore, CA, 1989.

Kerstein, A.R., *J. Fluid Mech.,* 231, pp. 361−394, 1991.

Masri, A.R. and Dibble, R.W., Twenty−Second Symposium (International) on Combustion, The Combustion Institute, Pittsburgh, PA, 1989, pp. 607−618.

Masri, A.R., Dibble, R.W., and Barlow, R.S., Twenty−Fourth Symposium (International) on Combustion, The Combustion Institute, Pittsburgh, PA, 1992, pp. 317−324.

Mauβ, F., Keller, D., and Peters, N., Twenty−Third Symposium (International) on Combustion, The Combustion Institute, Pittsburgh, PA, 1990, pp. 693−698.

Meyers, R.E. and O'Brien , E.E., *Combust. Sci. and Tech.* 26:123−134 (1981).

Norris, A.T. and Pope, S.B.,"Modeling of Extinction in Turbulent Diffusion Flames by the Velocity− Dissipation−Composition PDF Method," submitted to Twenty−Fifth Symposium (International) on Combustion, Irvine, CA, July 31−August 5, 1994.

Peters, N., Twenty−First International Symposium on Combustion, The Combustion Institute, Pittsburgh, PA, pp. 1231−1250, 1988.

Pope, S.B., *Comb. Sci. and Tech.,* 28: 131−145 (1982).

Pope, S.B., *Prog. Energy and Comb. Sci.,* 11, pp. 119−192, 1985.

Pope, S.B., Twenty−Third Symposium (International) on Combustion, The Combustion Institute, Pittsburgh, PA, pp. 591−612, 1990.

Pope, S.B., *Ann. Rev. Fluid Mech.*, 26, pp. 23−63, 1994.

Seshadri, K and Peters, N., *Comb. and Flame, 81,* pp. 96−118, 1990.

Smooke, M.D., private communications, 1993.

Smooke, M.D. and Giovangigli, V.,"Premixed and Nonpremixed Test Problem Results," in *Reduced Kinetic Mechanisms and Asymptotic Approximations for Methane−Air Flames*, (Smooke, M.D., Ed.), Springer, Lecture Notes in Physics Vol. 384, pp. 29−47, 1990.

Smith, N.S.A., Bilger, R.W., and Chen, J.−Y., Twenty−Fourth Symposium (International) on Combustion, The Combustion Institute, Pittsburgh, PA, 1992, pp. 263−269.

Spalding, D.B.,"Concentration Fluctuations in a Round Turbulent Free Jet," *J. Chem. Eng. Sci.* 26, pp. 95−107, 1971.

Taing, S., Masri, A.R., and Pope, S.B., *Combust. Flame,* 95, pp. 133−150, 1993.

Westbrook, C.K. and Dryer, F.L., *Comb. Sci. Tech., 27,* p. 31, 1981.

Section 5
WRITTEN PUBLICATIONS

This report is not comprehensive in terms of the details of the work that was performed. Additional description may be found in the several refereed reports that were produced as a result of this contract.

Refereed publications based on work performed in and written during the reporting period were:

1. Correa, S.M. and Pope, S.B.,"Comparison of a Monte–Carlo PDF/Finite–Volume Mean Flow Model with Bluff–Body Raman Data," Twenty–Fourth Symposium (International) on Combustion, The Combustion Institute, Pittsburgh, PA, pp. 279–285, 1992.

2. Correa, S.M.,"Turbulence–Chemistry Interactions in the Intermediate Regime of Premixed Combustion," *Comb. and Flame,* 93, pp. 41–60, 1993.

3. Correa, S.M., and Braaten, M.E.,"Parallel Simulations of Partially–Stirred Methane Combustion," GE Class I Report 92CRD273, November 1992; *Comb. and Flame,* 94, pp. 469–486, 1993.

4. Correa, S.M.,"Models for High–Intensity Turbulent Combustion," *Computing Systems in Engineering,* Vol. 5, No. 2, pp. 135–145, 1994.

5. Correa, S.M.,"Assessment of a 3–Variable Reduced Kinetic Scheme in Prescribed Turbulence," in press *J. Prop. Power,* 1994.

6. Correa, S.M., Gulati, A., and Pope, S.B.,"Raman Measurements and Joint PDF Modeling of a Non–Premixed Bluff Body–Stabilized Methane Flame," Twenty–Fifth Symposium (International) on Combustion, Irvine, CA, July 31 – August 5, 1994.

7. Correa, S.M. and Dean, A.J.,"Turbulent Broadening of Autoignition Limits," Twenty–Fifth Symposium (International) on Combustion, Irvine, CA, July 31 – August 5, 1994.

8. Correa, S.M.,"A Direct Comparison of Pair–Exchange and IEM Models in Premixed Combustion," submitted to *Comb. and Flame,* April 1994.

Section 6
PROFESSIONAL PERSONNEL

Dr. Sanjay M. Correa (PI), Dr. Mark E. Braaten, and Ms. Janet Sober worked on this program. Dr. Iris Hu became a member of the team in the last few months of the program.

Section 7
INTERACTIONS/TECHNOLOGY TRANSFER

The computational technology developed in the program has been widely disseminated in the archival literature and in invited talks and seminars, and elements of it are used in 3D CFD models of combustors. The measurements provide corroborating data not only for the models developed here but also for others. The research has also provided techniques for laser probing of practical combustors, e.g., multi–cup sectors are now being probed with Raman spectroscopy. Since we have shown that the computational methods developed in this research program can be fielded within the CFD codes used in design, ongoing transfer of the new research is assured.

Section 8
INVENTIONS

There were no inventions in the reporting period.